HYPERVELOCITY IMPACT ANALYSIS BY THE METHOD OF CHARACTERISTICS

by Richard Madden

Langley Research Center
Langley Station, Hampton, Va.

NATIONAL AERONAUTICS AND SPACE ADMINISTRATION • WASHINGTON, D. C. • JANUARY 1969

NASA TR R-298

HYPERVELOCITY IMPACT ANALYSIS BY THE METHOD OF CHARACTERISTICS

By Richard Madden

Langley Research Center
Langley Station, Hampton, Va.

NATIONAL AERONAUTICS AND SPACE ADMINISTRATION

For sale by the Clearinghouse for Federal Scientific and Technical Information
Springfield, Virginia 22151 – CFSTI price $3.00

HYPERVELOCITY IMPACT ANALYSIS BY THE METHOD OF CHARACTERISTICS

By Richard Madden
Langley Research Center

SUMMARY

A computer method has been developed for the analysis of the initial hydrodynamic phase of hypervelocity impact. The method is based on solving the inviscid, non heat-conducting, unsteady fluid dynamic equations in cylindrical coordinates by utilizing an approach based on the method of characteristics. The method has been used to generate an operational computer program applicable to the impact of an infinitely long right circular cylinder striking a semi-infinite target of the same material. The projectile is assumed to be traveling parallel to its axis of symmetry, and the target is initially at rest. Results are presented for the pressure and velocity fields at various times following the impact. The pressure fields are compared with the pressure fields calculated from an existing hydrodynamic analysis.

INTRODUCTION

The early stages of hypervelocity impact are characterized by shock waves in both the projectile and target materials with associated high pressures and internal energies. These extreme conditions justify the use of a hydrodynamic model for this portion of the impact. The hydrodynamic model has been customarily analyzed by using large-scale computer programs based on the particle in cell, or P.I.C., approach (ref. 1) or on a continuous Eulerian extension of the P.I.C. approach (ref. 2). These approaches divide the flow field into cells and determine average values of the dependent variables (pressure, internal energy, etc.) over the cells. A disadvantage of the averaging procedure is that it causes numerical diffusion because discontinuities, such as shocks and rarefactions, are smeared over a number of cells. Thus, the items of prime concern are treated in a numerically undesirable fashion. These disadvantages have been overcome by utilizing a numerical solution based on the method of characteristics. The practical implementation of this method to a numerical solution is not, however, straightforward for problems involving more than two independent variables.

The purpose of the present paper is to describe the development of a practical numerical solution of the hydrodynamic equations by using the method of characteristics

and to discuss some of the techniques which were utilized to obtain an operational computer program. The method determines values of the dependent variables directly, at discrete points in the flow field, and the major discontinuities present in the flow field are located at each time step in the numerical calculation. This knowledge is used to develop a procedure which insures that linear interpolation relations and spatial finite difference relations are not applied across a discontinuity. For the discontinuities considered, the numerical diffusion is essentially eliminated.

In the present approach it is not possible to make a priori statements concerning the stability of the numerical procedure. However, the bicharacteristics have been selected such that they best represent the conoid of dependence of the point under consideration; thus, the probability of encountering a numerical instability is reduced. Although the stability of the procedure has not been verified mathematically, the numerical results give no indication of stability difficulties. The actual FORTRAN computer program utilized in the present approach is discussed in reference 3.

SYMBOLS

A coefficient in equation of state

a coefficient in equation of state

B coefficient in equation of state

b coefficient in equation of state

c speed of sound

E internal energy

E_S sublimation energy

E_* coefficient in equation of state

F function defining regions

h time step

$l_O = \cos \psi$

$m_o = \sin \psi$

p pressure

R radius of projectile

r radial coordinate

t time

T elapsed time since impact

U shock velocity

u radial velocity

$\bar{u}$ velocity normal to shock

V initial velocity of projectile

v axial velocity

$\bar{v}$ velocity tangential to shock

z axial coordinate

α coefficient in equation of state

β coefficient in equation of state

ζ coordinate tangential to shock

$\eta = \frac{\rho}{\rho_*}$

θ angle between normal to characteristic surface and r-axis

$\bar{\theta} = \theta - \psi$

λ multiplier

$\mu = \eta - 1$

ξ coordinate normal to shock

ρ mass density

ρ_* undisturbed mass density

ψ angle between normal to shock and r-axis

Subscripts:

i ith bicharacteristic

o point in new time plane

p particle

s conditions ahead of shock

GOVERNING EQUATIONS

The initial stages of hypervelocity impact are characterized by very high pressures and very high internal energies. These extreme conditions allow the early stages to be analyzed by using a hydrodynamic model for the penetration process. (See, for example, ref. 2.) The present paper considers the initial deformation phase of a semi-infinite medium impacted by an infinitely long right circular cylinder. The cylinder and half-space are assumed to be of the same material. The problem as described is governed by the following classical, inviscid, non heat-conducting, Eulerian fluid dynamic equations with cylindrical symmetry:

conservation of mass

$$\frac{D\rho}{Dt} + \rho\left(\frac{\partial u}{\partial r} + \frac{\partial v}{\partial z} + \frac{u}{r}\right) = 0 \tag{1a}$$

conservation of radial momentum

$$\rho \frac{Du}{Dt} + \frac{\partial p}{\partial r} = 0 \tag{1b}$$

conservation of axial momentum

$$\rho \frac{Dv}{Dt} + \frac{\partial p}{\partial z} = 0 \tag{1c}$$

conservation of entropy along a particle path

$$\frac{Dp}{Dt} - c^2 \frac{D\rho}{Dt} = 0 \tag{1d}$$

where

$$\frac{D}{Dt} = \frac{\partial}{\partial t} + u \frac{\partial}{\partial r} + v \frac{\partial}{\partial z}$$

ρ is density, u and v are radial and axial velocities, respectively, p is pressure, c is speed of sound, r and z are radial and axial coordinates, respectively, and t is time.

Initial and Boundary Conditions

For the problem under consideration, the initial conditions are that the infinitely long cylindrical projectile is moving along its axis of symmetry at a velocity V and the semi-infinite target is at rest (fig. 1). The thermodynamic state variables (pressure and internal energy) are assumed to be zero everywhere and the density is assumed to be undisturbed everywhere.

The boundary conditions are that the radial velocity is zero on the axis of symmetry and the pressure is zero on the free surfaces of the projectile and target. The additional boundary conditions required to obtain a solution are applied on the low-pressure side of the shocks. In the present problem these conditions are that for both shocks the pressure and internal energy are zero, the density is undisturbed, and the velocity is equal to zero in the target and is equal to the impact velocity in the projectile. The boundary conditions are illustrated in figure 1(b) which shows a section taken through the axis of symmetry of figure 1(a).

Equation of State

The Tillotson equations of state (for either the compression region or the expansion region) from reference 4 have been used to describe the thermodynamic behavior of the materials. These equations may be written as follows:

$$p = \left(a + \frac{b}{\frac{E}{E_* \eta^2} + 1} \right) E\rho + A\mu + B\mu^2 \qquad \left(\rho > \rho_* \text{ with } 0 < E < E_s \right) \tag{2a}$$

and

$$p = aE\rho + \left(\frac{Eb\rho}{\frac{E}{E_* \eta^2} + 1} + A\mu e^{-\beta\left(\frac{1}{\eta} - 1\right)} \right) e^{-\alpha\left(\frac{1}{\eta} - 1\right)^2} \qquad \left(\rho < \rho_* \text{ with } E > E_S\right) \tag{2b}$$

where $\eta = \frac{\rho}{\rho_*}$, $\mu = \eta - 1$, and E_S is the sublimation energy.

GENERAL METHOD OF ANALYSIS

Since in many problems it is desirable to obtain a more refined numerical representation of the flow field than may be obtained from the usual P.I.C. type of approach (refs. 1 and 2), it was decided to attack the problem by using an approach based on the method of characteristics in three independent variables. The hyperbolic nature of the equations makes them ideally suited for solution by the method of characteristics. This method allows discontinuities to be preserved and additionally permits the calculation of dependent variables at discrete points in the flow field.

Characteristic Equations

The characteristic equations are determined from the original partial differential equations (eqs. 1(a) to 1(d)) in appendix A. The final form of these equations, which replace equations (1), is taken from the appendix as follows:

Slope equations along

Bicharacteristics

$$\frac{dr}{dt} = u + c\cos\theta \qquad \frac{dz}{dt} = v + c\sin\theta \tag{3a}$$

Particle paths

$$\frac{dr}{dt} = u \qquad \frac{dz}{dt} = v \tag{3b}$$

Compatibility equations along

Bicharacteristics

$$dp + \rho c\, du\cos\theta + \rho c\, dv\sin\theta = -\rho c^2 \left[\frac{\partial u}{\partial r}\sin^2\theta - \left(\frac{\partial u}{\partial z} + \frac{\partial v}{\partial r} \right)\sin\theta\cos\theta + \frac{\partial v}{\partial z}\cos^2\theta + \frac{u}{r} \right] dt \tag{3c}$$

Particle paths

$$dE = \frac{p}{\rho^2} d\rho \tag{3d}$$

where θ is the angle between the normal to the bicharacteristic and the r-axis. These equations are highly complex since in addition to the total differentials there are also spatial partial derivatives. The solution of these equations must therefore rely on numerical techniques based on finite difference forms of the characteristic equations.

Characteristic Equations in Numerical Form

The original characteristic equations (3) have been approximated by using finite difference relations as follows:

Slope equations along

Bicharacteristics

$$r_i = r_o - h\left(u_i + c_i \cos \theta_i\right) \tag{4a}$$

$$z_i = z_o - h\left(v_i + c_i \sin \theta_i\right) \tag{4b}$$

Particle paths

$$r_p = r_o - hu_p \tag{4c}$$

$$z_p = z_o - hv_p \tag{4d}$$

Compatibility equations along

Bicharacteristics

$$p_o - p_i + \rho_i c_i\left(u_o - u_i\right)\cos \theta_i + \rho_i c_i\left(v_o - v_i\right)\sin \theta_i = -\rho_i c_i^2 h \left[\left(\frac{\partial u}{\partial r}\right)_i \sin^2\theta_i - \left(\frac{\partial u}{\partial z} + \frac{\partial v}{\partial r}\right)_i \sin \theta_i \cos \theta_i + \left(\frac{\partial v}{\partial z}\right)_i \cos^2\theta_i + \frac{u_i}{r_i}\right] \tag{4e}$$

Particle paths

$$E_o - E_p = \frac{p_p}{\rho_p^2}\left(\rho_o - \rho_p\right) \tag{4f}$$

where the subscript i refers to values in the previous time plane associated with the bicharacteristic used and the subscript o refers to the point in the new time plane at which the solution is desired. The variables with subscript p refer to the particle located at (r_p,z_p) in the previous time plane and which now resides at (r_o,z_o). (See fig. 2.) Note that equations (4e) contain only three unknowns $(p_o,\ u_o,$ and $v_o)$ at some new point in time and that a numerical solution of equations (4e) along three bicharacteristics is both necessary and sufficient for a unique numerical solution of these unknowns. These equations are solved for $p_o,\ u_o,$ and v_o to yield values on a spatial grid superimposed on the flow field at each increment in time.

Approximate Initial Conditions

At the initial instant of impact ($T = 0$), conditions are specified on the surface; that is, $z = 0,\ r > R$. If the bicharacteristic slope and compatibility conditions could be integrated exactly, these initial data would be sufficient to determine the solution for any (r,z,t). The numerical procedure for the method of characteristics problem discussed herein utilizes more than two bicharacteristics and consequently requires initial data specified over some volume in the r,z space.

Thus, some procedure is required to convert the initial conditions on the surface at $T = 0$ to a spatial set of initial conditions. This conversion was accomplished by advancing out the solution for some small time by an approximate technique. The resulting solution is then used as initial data for the characteristic solution in three independent variables. In this analysis the initial data are generated by considering the impact to be one-dimensional in the region directly beneath the projectile and in the compressed region of the projectile. These values are obtained directly from the solution of a one-dimensional impact. Values in the region $r > R$ near the corner of the projectile are obtained by allowing the shock to advance spherically from the corner with a radius equal to the maximum depth of penetration of the target shock. The velocity of each particle in this region is assumed to be equal to the particle velocity in the one-dimensional region; however, it is now directed radially from the point $(R,0)$ to the particle.

The rarefaction proceeding in from the free edges of the projectile is also included. The location of the rarefaction is determined from a spherical wave traveling at the speed of sound in the compressed material and whose center is at $\left(R,\frac{VT}{2}\right)$. Values for all variables on the shocks, the shock location, and the rarefaction location are now known. Values for the interior points between the axis of symmetry and the rarefaction are the one-dimensional values, and points between the rarefaction and the free boundary are assigned values obtained by linear interpolation between the values on the free boundary and the one-dimensional values on the rarefaction. The values on the free boundary are

found by setting the pressure and internal energy equal to zero and the density equal to the undisturbed density ρ_*.

The present procedure for establishing initial conditions conserves neither momentum nor energy. However, if the radius of the projectile is large and the time step is small, the error introduced by the scheme is negligible.

Approximate Boundary Conditions

The boundary conditions are taken to be that the radial velocity is zero on the axis of symmetry and that the pressure vanishes along the original free surfaces of both the projectile and the target ($r = R, \quad z < 0$ and $z = 0, \quad r \geq R$). These pressure boundary conditions are not strictly correct because there is motion of the free surfaces and, consequently, the actual free surface does not coincide with the original free surface except at $T = 0$. This procedure was used for convenience; the actual condition of a moving free surface could be handled by using the same location techniques as used for the shocks at the expense of a more complicated computer program. However, for the early stages of hypervelocity impact this approximation appears to be reasonable.

NUMERICAL ANALYSIS

Topological Aspects

The numerical solution of equations (4) is complicated because physical discontinuities (shocks and rarefactions) appear in the flow field. Finite difference approximations are meaningful only when the differenced function is continuous over the finite difference interval. Therefore care must be taken to insure that finite difference relations are not applied across discontinuities. However, the discontinuities (shocks and rarefactions) divide the flow field into specific identifiable regions within which a numerical solution is valid. Thus all calculations which relate to a point in a given region may be required to use information from points within that region. Consequently, numerical diffusion (smearing out of discontinuities) is essentially eliminated for those discontinuities considered herein. The procedure for minimizing numerical diffusion is discussed more generally in the following sections.

Discontinuities and Particle Curves

The procedure for minimizing diffusion requires locating the discontinuities at each time cycle. The discontinuities utilized in this analysis are as follows:

(1) Projectile shock

(2) Projectile-shock particle curve

(3) Target shock

(4) Target-shock particle curve

(5) Rarefaction

(6) Rarefaction particle curve

It is obvious that the shocks and rarefaction are locations of discontinuities. The additional discontinuities which are defined herein as particle curves are the locus of all particles in the new time plane which were located on a given discontinuity in the old time plane. These curves must be defined since all particles which lie between this curve and the discontinuity in the new time plane have undergone discontinuous behavior during the time step. Consequently, the finite difference relations (4c), (4d), and (4f) written over the time step for any of these particles are meaningless. In this region, however, it is still possible to solve equations (4a), (4b), and (4e) to determine p_o, u_o, and v_o.

This set of six discontinuities does not encompass all the discontinuities actually present in the physical situation. For instance, the reflection of a rarefaction from a shock or from the axis of symmetry is neglected. Discontinuities of this type have been neglected either because they are known to be weak or because they are not of major interest in hypervelocity impact problems. The neglect of these interactions as discontinuities does not remove them from the solution; however, it does allow them to be diffused throughout the flow field.

Classification of Regions

To categorize the behavior at a point in space, it is convenient to assign each point in the flow field to a particular region. The regions are shown in figure 3 and are defined as follows:

Region I – Outside the target shock

Region II – Outside the projectile shock

Region III – Between the target shock and target-shock particle curve

Region IV – Between the projectile shock and the projectile-shock particle curve

Region V – Between the rarefaction and rarefaction particle curve

Region VI – Outside the projectile and target

Region VII – Between the rarefaction particle curve, the particle curves for the two shocks, and the free boundary

Region VIII – Between the rarefaction, the particle curves for the two shocks, and the axis of symmetry

Separation of the flow field in this manner defines the regions in which values of the dependent variables may be calculated.

In regions I, II, and VI, calculations are unnecessary since the material in these regions is undisturbed. In regions III, IV, and V, calculations for density and internal energy may not be performed since the finite difference relation for the particle path equation is not applicable over the entire time step. Calculations for pressure and velocity may be performed since the bicharacteristics are not discontinuous. However, for convenience, values of all dependent variables between the discontinuity and particle curves are obtained by interpolation between calculated values on the discontinuity and calculated values on an adjacent grid point behind the particle curve. In region VIII, calculations are unnecessary since the values of all dependent variables remain the same as the one-dimensional input values. In region VII, calculations are performed by using the procedures to be outlined in a subsequent section.

Differentiation of Regions

Each of the discontinuities at any time is specified by a given number of points. Between two successive points on the discontinuity a straight line may be constructed. This line has an equation of the form

$$r = a_1 z + a_2 \quad \text{or} \quad z = a_3 r + a_4$$

where $a_1 \ldots a_4$ are arbitrary constants. If these equations are written in a functional form $F(r,z)$ such as

$$F(r,z) = r - a_1 z - a_2 \tag{5a}$$

or

$$F(r,z) = z - a_3 r - a_4 \tag{5b}$$

certain properties can be recognized. In particular, on the discontinuity F is zero, and on one side of the discontinuity F is positive and on the other side F is negative.

This property may best be illustrated by the following two examples. First, straight lines through rarefaction points are in the form of equation (5a). To determine whether a given point has been affected by the rarefaction, a straight line is constructed between the two closest rarefaction points and then F is evaluated. A value of F greater than zero indicates that the point has been affected by the rarefaction. Second, straight lines through shock points are in the form of equation (5b). To determine whether a given point lies outside the target shock, a straight line is constructed between the two closest target shock points and then F is determined. A value of F greater than zero indicates that the point is outside the target shock.

SOLUTION OF FINITE DIFFERENCE EQUATIONS

The finite difference equations are solved at each time plane to yield values of the dependent variables on the projectile and target shocks and also at points on a rectangular grid superimposed on the flow field. The solution of the equations at various locations in the flow field requires the consideration of two classes of points: those points that lie sufficiently far away from a discontinuity (shock or rarefaction) and hence have a full conoid of dependence and those points that lie on or near a discontinuity and therefore have a partial conoid of dependence. The numerical representation of the equations and the procedures for handling these two classes of points are discussed in the following sections. A discussion of the stability of the numerical scheme is given in appendix B. The actual calculation procedure and a detailed analysis of the computer program with FORTRAN listing are presented in reference 3.

Points Having a Full Conoid of Dependence

For points having a full conoid of dependence, three bicharacteristics are required to approximate the conoid. The values for θ_i are chosen, equally spaced, to be 0, $2\pi/3$, and $4\pi/3$. The values of θ_i are chosen from stability considerations. (See appendix B.) The calculation requires the choice of a point (r_o,z_o) at which the solution is desired in the new time plane. The location (r_i,z_i) in the previous time plane of the bicharacteristics which pass through (r_o,z_o) may then be determined from equations (4a) and (4b). It is possible to find a point (r_i,z_i) for which u_i, v_i, and c_i satisfy equations (4a) and (4b) since values of all dependent variables are specified on the grid and on the discontinuities in the previous time plane. However, the solution of equations (4a) and (4b) is complicated by the fact that there is no explicit relation tying (r_i,z_i) to (u_i,v_i,c_i) in a given time plane. It is therefore necessary to choose some trial location for a bicharacteristic (r_i,z_i) and use an iterative procedure (such as the Newton-Raphson method) to determine the actual coordinates r_i and z_i. Once the coordinates r_i and z_i are established, interpolation is performed between the four surrounding grid points (or discontinuities) in the rz-plane to determine the values for all the required dependent variables at (r_i,z_i). Partial derivatives with respect to r and z at (r_i,z_i) are evaluated by using a forward or backward difference scheme. The three linear difference equations (4e) are then solved simultaneously to give p_o, u_o, and v_o at (r_o,z_o). Equations (4c) and (4d) are then solved to determine the location in the previous time plane (r_p,z_p) of the particle which now resides at (r_o,z_o). Interpolation for dependent variables at (r_p,z_p) is performed and the values for ρ_o and E_o are obtained from equation (4f) and the equations of state (2) by using an iterative procedure such as the

Newton-Raphson method. The speed of sound, at this point, may be obtained by differentiating the appropriate equation of state as follows:

$$c^2 = \left(\frac{\partial p}{\partial \rho}\right)_E + \frac{p}{\rho^2}\left(\frac{\partial p}{\partial E}\right)_\rho \tag{6}$$

Points Having a Partial Conoid of Dependence

Points lying near a discontinuity.- Points having a partial conoid of dependence which lie near, but not on, a discontinuity are handled in almost the same manner as points having a full conoid of dependence. The only difference is that a new set of three bicharacteristics θ_i must be chosen to insure that none of the bicharacteristics cross the discontinuity. The bicharacteristics θ_i are established by a search technique which finds the intersection of the discontinuity and the conoid and then divides the remaining conoid into four equal angles. The computer program has a special routine which chooses the best set of bicharacteristics in this case.

Points lying on a discontinuity.- The approach using three bicharacteristics is not required for points having a partial conoid of dependence which lie on a discontinuity since auxiliary relations or specified values of the dependent variables at these points supply sufficient information to form a complete set of equations. The particular procedures applicable for each of these types of points are discussed separately.

Points on the axis of symmetry: For points on the axis of symmetry, the radial velocity u vanishes ($u = 0$) and therefore only two bicharacteristics are required rather than the usual three. The two bicharacteristics θ_i chosen to be the best approximation of the conoid are $2\pi/3$ and $4\pi/3$. The solution of equations (4a) and (4b) for the two bicharacteristics is accomplished in the same manner as discussed for points having a full conoid of dependence. However, u_o is set equal to zero in equations (4e) leaving only two variables p_o and v_o. The determination of ρ_o and E_o is performed in the same manner as explained in the section entitled "Points Having a Full Conoid of Dependence."

Points on a free boundary: For points on a free boundary, the pressure p_o is equal to zero and again only two bicharacteristics are required. The choice of bicharacteristics that lie in the flow field depends on whether the free boundary is along an r or z grid line. If $r = R$ is the free boundary, the two bicharacteristics $\theta_i = \frac{\pi}{3}$ and $\frac{5\pi}{3}$ are chosen; whereas, if the boundary is along $z = 0$, the appropriate bicharacteristics are $4\pi/3$ and $5\pi/3$. In the solution of equations (4e) the value of p_o is set equal to zero. To maintain $p_o = 0$ on the free surfaces with the present equation of state, it was

assumed that the specific internal energy was zero (E = 0) and that density was undisturbed ($\rho = \rho_*$).

Points on a shock wave: Points on a shock wave do not possess a full conoid of dependence since values of the dependent variables at these points can depend only on values at points encompassed by the shocks. The method employing three bicharacteristics is not required inasmuch as additional relations are available from the conservation laws expressed across the shocks. The procedure described for solving the equations is similar to that developed in reference 5.

The conservation relations across the shock and the equation of state provide four equations in the five unknowns and therefore only one bicharacteristic relation is required to form a complete set.

For shock-wave calculations a set of local orthogonal coordinates ξ, ζ is used at each point on the shock front. The coordinate ξ is defined as the normal to the shock taken in the direction of motion, and the shock and the coordinate ζ form a right-hand coordinate system with it. The ξ-axis forms an angle ψ with the original r-axis. The desired bicharacteristic is perpendicular to the shock and is $\bar{\theta} = 0$ where $\bar{\theta} = \theta - \psi$. These relationships are shown in the following sketch:

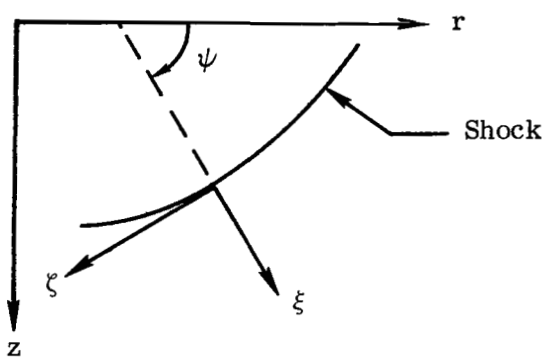

In this new set of axes, equation (3c) along a bicharacteristic becomes

$$dp + \rho c \cos \bar{\theta}\, d\bar{u} + \rho c \sin \bar{\theta}\, d\bar{v} = -\rho c^2 \bar{S}\, dt \tag{7}$$

where

$$\bar{S} = \frac{\partial \bar{u}}{\partial \xi} \sin^2 \bar{\theta} - \left(\frac{\partial \bar{u}}{\partial \zeta} + \frac{\partial \bar{v}}{\partial \xi} \right) \sin \bar{\theta} \cos \bar{\theta} + \frac{\partial \bar{v}}{\partial \zeta} \cos^2 \bar{\theta} + \frac{u}{r}$$

and

$$\bar{\theta} = \theta - \psi \qquad l_o = \cos\psi$$

$$\bar{u} = l_o u + m_o v \qquad m_o = \sin\psi$$

$$\bar{v} = l_o v + m_o u$$

Note that the last term in $\bar{S}$ contains an unbarred u. The finite difference equivalent of equation (7) with $\theta = \psi$ ($\bar{\theta} = 0$) becomes

$$p_o - p_1 + \rho_1 c_1 \left(\bar{u}_o - \bar{u}_1\right) = -\rho_1 c_1^2 h \left[\left(\frac{\partial \bar{v}}{\partial \zeta}\right)_1 + \frac{u_1}{r_1}\right] \tag{7a}$$

where the subscript 1 refers to the values at the point where the bicharacteristic ($\bar{\theta} = 0$) intersects the previous time plane. The characteristic slope equations are most conveniently used in the form of equations (4a) and (4b) with θ set equal to ψ. The additional equations required are as follows:

From conservation of mass and momentum across the shock,

$$\left(\bar{u}_b - \bar{u}_s\right)^2 = \left(p_b - p_s\right)\left(\frac{1}{\rho_s} - \frac{1}{\rho_b}\right) \tag{8}$$

and

$$U = \frac{\rho_b \bar{u}_b - \rho_s \bar{u}_s}{\rho_b - \rho_s} \tag{9}$$

where the subscript s refers to conditions ahead of the shock and the subscript b refers to conditions just behind the shock.

From the Rankine-Hugoniot relations,

$$E_b - E_s = \frac{1}{2}\left(p_b + p_s\right)\left(\frac{1}{\rho_s} - \frac{1}{\rho_b}\right) \tag{10}$$

From the constancy of tangential velocity across the normal discontinuity (shock),

$$\bar{v}_b = \bar{v}_s \tag{11}$$

Equation (7a) is now combined with equation (8), after setting $p_s = 0$, to obtain the following equation which is more amenable to solution:

$$p_b + \rho_1 c_1 \left[\bar{u}_s \pm \sqrt{p_b \left(\frac{1}{\rho_s} - \frac{1}{\rho_b} \right)} \right] = -\rho_1 c_1^2 h \left[\left(\frac{\partial \bar{v}}{\partial \zeta} \right)_1 + \frac{u_1}{r_1} \right] + p_1 + \rho_1 c_1 \bar{u}_1 \tag{12}$$

where the positive square root is used in target shock calculations $(\bar{u}_s = 0)$ and the negative square root is used in projectile shock calculations $(\bar{u}_s = V)$.

Equations (10) and (12) are solved with $p_s = 0$ by using an iterative procedure, such as the Newton-Raphson method, to obtain ρ_b and E_b. The pressure p_b in these equations is obtained from the equation of state (2a). The speed of sound may now be obtained from equation (6), and the velocity normal to the shock $\bar{u}_b$ is obtained from equation (8).

RESULTS AND DISCUSSION

The particular example chosen to illustrate the results of the characteristic approach is the impact of an infinitely long cylindrical aluminum projectile 2.5 cm in diameter on an aluminum half-space. The initial velocity of the projectile is taken to be 7.6 km/s and the half-space is assumed to be at rest. Initially, a 0.125-cm-square grid is used; however, a grid change is made at $T = 1.20$ μs and thereafter the grid becomes a 0.25-cm-square grid. The Tillotson equations of state (ref. 4) are used to define the thermodynamic behavior of the aluminum.

Pressure fields and velocity fields from the characteristic method are illustrated at $T = 0.74$ μs, $T = 1.26$ μs, and $T = 1.50$ μs. Also presented are a plot of pressure on the axis of symmetry as a function of time and a plot of discontinuity location as a function of time. The pressure plots are compared with the results from the well-known OIL computer program of reference 2. Results from the OIL program have been compared extensively with exact solutions and therefore are a logical choice for comparison herein.

Pressure Fields

Figure 4 gives the pressures on the axis of symmetry at a time before reflection of the rarefaction from the axis of symmetry ($T = 0.74$ μs), obtained by both the method of characteristics and the OIL approach. Since the discontinuities have been tracked, the characteristic method predicts the exact hydrodynamic behavior, that is, a one-dimensional region bounded by two sharp shocks. The OIL approach, on the other hand, has numerical diffusion near the shocks. It is noted also that the OIL method tries to

compensate for the smearing by admitting a pressure directly behind the shock which is higher than the one-dimensional value.

Figure 5 shows the pressure distributions in the entire flow field for both solutions at $T = 0.74$ μs. These distributions are compared by plotting isobars for $p = 1.08$, 0.8, 0.5, and 0.2 Mb (108, 80, 50, and 20 GN/m^2). (Note that 1 Mb = 100 GN/m^2.) The method of characteristics distributions are shown as solid lines and the OIL distributions as dashed lines. The locations of the two shocks and the rarefaction are clearly defined for the characteristic method. One difference immediately apparent between the two sets of isobars is that the isobars for the OIL approach begin and end on the axis of symmetry, whereas the isobars for the characteristic method begin and end on the shocks. This difference, of course, comes from the smearing of shocks in the OIL solution. The OIL approach additionally predicts two regions of pressures higher than the one-dimensional region bounded by the two shocks and the rarefaction ($p = 1.08$ Mb). The reduction of pressure in the rarefied region is predicted, similarly, by both methods. Agreement of the isobars for $p = 0.8$ Mb is good except near the shocks. The isobars for $p = 0.5$ and 0.2 Mb also compare quite favorably with major differences noted near the free surface, where pressures are low. In general, the results of the two methods are in agreement. However, the absence of diffusion in the characteristic method results in a more accurate solution at any point.

The pressure fields for both the characteristic and OIL approaches at $T = 1.26$ μs are shown in figure 6. At this time a portion of the rarefaction has been reflected from the axis of symmetry. Again, the trends for both approaches are in agreement. The difference between the isobars for $p = 0.5$ Mb in the central portion of the flow field is caused, in part, by the low pressure between the shocks computed by the OIL approach (fig. 4).

Figure 7 illustrates the isobars as predicted by both approaches at $T = 1.5$ μs. The isobars again compare favorably. Considering the characteristic method results, the higher pressure isobars for the earlier flow stage were seen to follow the shape of the rarefaction. However, for this time and for succeeding stages in the flow the higher pressure isobars follow a different pattern. In particular, these isobars turn outward in the central region of the flow field; this indicates that the pressure is higher than might be expected from an extrapolation of the behavior of the isobars at an earlier stage in the flow. This higher pressure results from the fact that as the projectile shock progresses it is attenuated and, therefore, particles passing through it are not decelerated as much. These particles enter the area between the projectile and target shocks with high velocities and must again be decelerated in the flow field. This additional deceleration gives rise to the increase in pressure.

Figure 8 presents pressure profiles on the axis of symmetry at three different times. The profile at $T = 1.26\ \mu s$ illustrates a completely one-dimensional behavior and is similar to the profiles that would be obtained for times before reflection of the rarefaction from the axis of symmetry. The next type of profile is shown at $T = 1.48\ \mu s$. At this time reflection of a portion of the rarefaction has occurred and gives an area in which the pressures are less than one-dimensional. However, the rarefaction has not completely reflected and therefore one-dimensional regions still remain adjacent to the shocks. The slope of the rarefaction near the projectile shock is greater than that near the target shock; this indicates that the rarefaction is much stronger near the projectile shock than near the target shock. This difference in strength is caused by the relative distances from the free surface. The profile at $T = 1.75\ \mu s$ illustrates the behavior following complete reflection of the rarefaction. At this time the entire profile is similar to the center portion of the profile for $T = 1.48\ \mu s$ and additionally the shocks have been attenuated to a pressure below the one-dimensional value.

Velocity Fields

The velocity vector field is shown in figure 9 for $T = 0.74\ \mu s$. Each arrow indicates both the magnitude and the direction of the velocity present at the tail of the vector. A vector of 7.6 km/s has been plotted below the flow field to establish the scale for the plot. The two shocks and the rarefaction are shown as solid lines. The vectors indicate that the area of the projectile unaffected by the shock has the original projectile velocity (7.6 km/s) and that the area between the shocks, rarefaction, and axis of symmetry is one-dimensional with a velocity equal to one-half the impact velocity. The velocity vectors are seen to turn radially outwards in the region outside the rarefaction. This change in direction results from the radial component imparted to the velocity vector when a point passes out of the rarefaction and from spherical divergence. The vectors indicate that there is a vortex-type flow as material slides along the target shock and moves upward through the original free surface, as evidenced by the negatively directed vectors near the target free surface. Some of this material eventually forms the lip which is commonly seen in impacted semi-infinite targets. The magnitude of the vectors illustrates that in the area near the rarefacted target shock, the velocity is less than the one-dimensional velocity and decreases radially along the shock. However, in the area of the projectile shock, velocities are above the one-dimensional value. This velocity increase results from the attenuation of the projectile shock strength and particles passing through the shock are not slowed greatly. In fact, near the projectile radius, where the projectile shock is strongly attenuated, some of the velocity vectors are 50 to 60 percent greater than the one-dimensional value.

Figures 10 and 11 illustrate the velocity vector fields at $T = 1.26\ \mu s$ and $T = 1.5\ \mu s$, respectively. Since the problem under consideration is the impact of an infinitely long projectile, the flow field is continually "fed" through the projectile shock and, consequently, the velocity vector plots have similar characteristics for all times. The only differences are in the continued "vortex" activity and the increased magnitude of the vectors near the projectile shock. In fact, the velocities near the intersection of the projectile shock and the free surface are just slightly reduced from the original projectile velocity.

Discontinuity Locations

In figure 12 the location of the discontinuities is shown as a function of time. The behavior of the rarefaction may be determined independently from that of the shocks since the rarefaction always proceeds toward the axis of symmetry as a toroidal segment with its center at the point $\left(r,z = R,\frac{VT}{2}\right)$.

The shocks are seen to be straight before arrival of the rarefaction. After arrival of the rarefaction the strength of the target shock decreases and the shock normal turns radially. After the passage of less than 1 μs the shock velocity has been reduced to approximately the speed of sound in the uncompressed material. Since the velocity of the material in front of the target shock is zero, this shock always advances in the same direction. The projectile shock, however, behaves a little differently since the position of a projectile shock point is governed by both its local shock velocity and the impact velocity. At this impact velocity a projectile shock point, therefore, advances in the negative z-direction until its local shock velocity is attenuated to a value below the original projectile velocity. Thereafter, the point travels in a positive z-direction. This motion can be seen by observing the projectile shock point closest to the free surface.

CONCLUDING REMARKS

A numerical method of analysis for determining the initial hydrodynamic phase of the axisymmetric impact of an infinitely long right circular cylindrical projectile on a semi-infinite target has been developed and programed. This method, based on the method of characteristics in three independent variables, differs from other approaches currently in use, such as the particle in cell (P.I.C.) method, in that specific values may be obtained at any point in the flow field directly rather than by integrating over some finite volume. The method keeps track of the locations of the major discontinuities, such as the shocks and rarefaction, at each time step and therefore essentially eliminates the numerical diffusion present in other numerical solutions to hydrodynamic behavior. Thus,

the shock-wave phenomenon, which is of prime interest, is not smeared out in the numerical calculation procedure.

The pressure fields obtained by using this numerical method of analysis have been compared with pressure fields obtained from the computer program based on a continuous Eulerian extension of the particle in cell approach (OIL) and good agreement is indicated when smearing of discontinuities inherent in the OIL program is disregarded. Of the two programs, OIL takes approximately one-tenth of the computer time of the characteristic solution; the additional time required by the method of characteristics is justified by the increased point-to-point accuracy. The techniques used in developing the characteristic solution should be valuable in other areas of fluid dynamics as well as hypervelocity impact.

Langley Research Center,
National Aeronautics and Space Administration,
Langley Station, Hampton, Va., July 10, 1968,
124-09-15-04-23.

APPENDIX A

METHOD OF CHARACTERISTICS

A brief description of the development of the characteristic slope and compatibility equations is presented. More general discussion of the method of characteristics and its applications to other fields is given in references 6 to 9.

Characteristic Slope Equations

The fluid dynamic equations (1) may be condensed to a convenient form by using "index notation" as follows:

$$a_{ijk} \frac{\partial \varphi_j}{\partial x_k} + b_i = 0 \tag{A1}$$

where φ_j represent the dependent variables, x_k represent the independent variables, and $a_{ijk} = a_{ijk}(\varphi_j)$ and $b_i = b_i(\varphi_j, x_k)$. The characteristic slope equations for equations (A1), most easily developed by changing the independent variables from x_k to some arbitrary coordinate system β_1, β_2, and β_3, are

$$a_{ijk} \frac{\partial \varphi_j}{\partial \beta_m} \frac{\partial \beta_m}{\partial x_k} + b_i = 0 \tag{A2}$$

With the assumption that values of all the dependent variables and their derivatives with respect to β_2 and β_3 are specified on a surface β_1 = Constant, these transformed partial differential equations would be expected to yield the derivatives with respect to β_1, if they exist. These derivatives are

$$a_{ijk} \frac{\partial \varphi_j}{\partial \beta_1} \frac{\partial \beta_1}{\partial x_k} = -b_i - a_{ijk} \frac{\partial \varphi_j}{\partial \beta_\alpha} \frac{\partial \beta_\alpha}{\partial x_k} \qquad (\alpha = 2,3) \tag{A3}$$

In developing the characteristic slope equations, however, it is desired to determine the conditions under which the derivatives normal to β_1 do not exist (normal derivatives to the surfaces, β_1 = Constant, are discontinuous). These surfaces are then called characteristic surfaces. The requirement for discontinuities in the derivatives with respect to β_1 is then the vanishing of the determinant of the coefficients of the derivatives with respect to β_1 in equations (A3); that is,

$$\det \left| a_{ijk} \frac{\partial \beta_1}{\partial x_k} \right| = 0 \tag{A4}$$

This condition always yields a set of slope equations; however, the β_1 surfaces correspond to physical surfaces only when these slopes are real, that is, when the original equations are hyperbolic or parabolic. For equations (1), equation (A4) takes the form

$$\begin{vmatrix} 0 & \frac{D\beta_1}{Dt} & \rho\frac{\partial\beta_1}{\partial r} & \rho\frac{\partial\beta_1}{\partial z} \\ \frac{\partial\beta_1}{\partial r} & 0 & \rho\frac{D\beta_1}{Dt} & 0 \\ \frac{\partial\beta_1}{\partial z} & 0 & 0 & \rho\frac{D\beta_1}{Dt} \\ \frac{D\beta_1}{Dt} & -c^2\frac{D\beta_1}{Dt} & 0 & 0 \end{vmatrix} = 0 \tag{A5}$$

Expanding the determinant gives

$$\rho^2\left(\frac{D\beta_1}{Dt}\right)^2\left\{-\left(\frac{D\beta_1}{Dt}\right)^2 + c^2\left[\left(\frac{\partial\beta_1}{\partial r}\right)^2 + \left(\frac{\partial\beta_1}{\partial z}\right)^2\right]\right\} = 0 \tag{A6}$$

where

$$\frac{D\beta_1}{Dt} = \frac{\partial\beta_1}{\partial t} + u\frac{\partial\beta_1}{\partial r} + v\frac{\partial\beta_1}{\partial z}$$

Equation (A6) has three possible solutions: the trivial solution $\rho = 0$ and two nontrivial solutions

$$\left(\frac{D\beta_1}{Dt}\right)^2 = 0 \tag{A7}$$

and

$$-\left(\frac{D\beta_1}{Dt}\right)^2 + c^2\left[\left(\frac{\partial\beta_1}{\partial r}\right)^2 + \left(\frac{\partial\beta_1}{\partial z}\right)^2\right] = 0 \tag{A8}$$

Equation (A7) may be investigated as a linear equation; however, for the sake of consistency in the mathematical analysis it is treated as a nonlinear equation. By expressing equation (A7) as

$$F = \left(\frac{\partial\beta_1}{\partial t} + u\frac{\partial\beta_1}{\partial r} + v\frac{\partial\beta_1}{\partial z}\right)^2 = 0 \tag{A9}$$

and applying the techniques from nonlinear partial differential equations (ref. 6), the characteristic slope equations become

$$\frac{dr}{d\nu} = \frac{\partial F}{\partial \beta_r} = 2\left(\beta_t + u\beta_r + v\beta_z\right)u$$

$$\frac{dz}{d\nu} = \frac{\partial F}{\partial \beta_z} = 2\left(\beta_t + u\beta_r + v\beta_z\right)v$$

$$\frac{dt}{d\nu} = \frac{\partial F}{\partial \beta_t} = 2\left(\beta_t + u\beta_r + v\beta_z\right)$$

where subscripts r, z, and t denote derivatives of β_1, and ν is a parameter. Eliminating the parameter ν gives

$$\frac{dr}{dt} = u \qquad \frac{dz}{dt} = v \tag{A10}$$

The characteristic slopes for equation (A7) are thus the particle paths which are surfaces of possible discontinuity in the entropy derivative.

Equation (A8) may be analyzed in an analogous fashion by redefining F to be

$$F = \left(\frac{\partial \beta_1}{\partial t} + u\frac{\partial \beta_1}{\partial r} + v\frac{\partial \beta_1}{\partial z}\right)^2 - c^2\left[\left(\frac{\partial \beta_1}{\partial r}\right)^2 + \left(\frac{\partial \beta_1}{\partial z}\right)^2\right] = 0 \tag{A11}$$

The characteristic slope equations therefore are

$$\frac{dr}{d\nu} = \frac{\partial F}{\partial \beta_r} = 2\left(\beta_t + u\beta_r + v\beta_z\right)u - 2c^2\beta_r$$

$$\frac{dz}{d\nu} = \frac{\partial F}{\partial \beta_z} = 2\left(\beta_t + u\beta_r + v\beta_z\right)v - 2c^2\beta_z$$

$$\frac{dt}{d\nu} = \frac{\partial F}{\partial \beta_t} = 2\left(\beta_t + u\beta_r + v\beta_z\right)$$

Eliminating the parameter ν gives

$$\frac{dr}{dt} = u - \frac{c^2\beta_r}{\beta_t + u\beta_r + v\beta_z}$$

$$\frac{dz}{dt} = v - \frac{c^2\beta_z}{\beta_t + u\beta_r + v\beta_z}$$

Using equation (A11) to reduce these equations yields

$$\left.\begin{aligned} \frac{dr}{dt} &= u \pm c \frac{\beta_r}{\sqrt{\beta_r{}^2 + \beta_z{}^2}} \\ \frac{dz}{dt} &= v \pm c \frac{\beta_z}{\sqrt{\beta_r{}^2 + \beta_z{}^2}} \end{aligned}\right\} \tag{A12}$$

Equations (A12) may be reduced to a more tractable form by noting that the direction cosines of the projection on the rz-plane of the normal to the surface $\beta_1 = \text{Constant}$ are

$$\cos\left(\beta_1, r\right) = \frac{\beta_r}{\sqrt{\beta_r{}^2 + \beta_z{}^2}}$$

$$\cos\left(\beta_1, z\right) = \frac{\beta_z}{\sqrt{\beta_r{}^2 + \beta_z{}^2}}$$

By defining

$$\left.\begin{aligned} -\cos\left(\beta_1, r\right) &= \cos\theta \\ -\cos\left(\beta_1, z\right) &= \sin\theta \end{aligned}\right\} \tag{A13}$$

the slope equations (A12) become

$$\left.\begin{aligned} \frac{dr}{dt} &= u \pm c\cos\theta \\ \frac{dz}{dt} &= v \pm c\sin\theta \end{aligned}\right\} \tag{A14}$$

In equations (A14) only the positive sign need be considered since the negative sign may be obtained by changing the reference for θ by π. The characteristic slope equations are then

$$\left.\begin{aligned} \frac{dr}{dt} &= u + c\cos\theta \\ \frac{dz}{dt} &= v + c\sin\theta \end{aligned}\right\} \tag{A15}$$

APPENDIX A

In equations (A15) a given value of the parameter θ (for $0 \leqq \theta \leqq 2\pi$) defines one of the characteristic directions at a point. These characteristics are termed "bicharacteristics." Considering the entire range of θ (for $0 \leqq \theta \leqq 2\pi$), equations (A15) describe a general cone in space called the characteristic conoid (fig. 13). The family of bicharacteristics are the generators of the conoid. In the $(t_o - h)$ plane, the conoid envelops an area termed "the domain of dependence" which encompasses all points which affect (r_o, z_o) at t_o. The point (r_o, z_o, t_o) is dependent only on the conditions which exist inside and on the conoid of dependence.

Compatibility Equations

A compatibility equation is a partial or total differential equation in which none of the indeterminable derivatives normal to β_1 exist – that is, it is an equation which is valid along the directions indicated by the characteristic slope equations.

Equations (A10) are recognized to be particle path equations and therefore there are many possible compatibility equations for this slope, for example, equations (1b), (1c), and (1d). However, for the present problem the first law of thermodynamics taken along the isentropic particle path

$$T\,ds = 0 = dE - \frac{p}{\rho^2}\,d\rho \tag{A16}$$

is the most useful (T being temperature and s being entropy).

The compatibility equation corresponding to the bicharacteristics given by equations (A15) is obtained by combining the transformed equations (1) in a manner such that the indeterminable derivatives (with respect to β_1) do not appear. This simplification is done most easily by multiplying equations (1a), (1b), (1c), and (1d) by weighting factors λ_1, λ_2, λ_3, and λ_4, respectively, and summing. Relations between the λ's are found by equating to zero the coefficients of the derivatives with respect to β_1 in the transformed equations. The derivatives can be written in the form

$$\lambda_i A_{ijk} \frac{\partial \beta_1}{\partial x_k} = 0$$

Applying this procedure gives

$$\left.\begin{aligned}
&\lambda_4 \frac{D\beta_1}{Dt} + \lambda_2 \frac{\partial \beta_1}{\partial r} + \lambda_3 \frac{\partial \beta_1}{\partial z} = 0 \\
&\lambda_1 \frac{\partial \beta_1}{\partial r} + \lambda_2 \frac{D\beta_1}{Dt} = 0 \\
&\lambda_1 \frac{\partial \beta_1}{\partial z} + \lambda_3 \frac{D\beta_1}{Dt} = 0 \\
&\lambda_1 \frac{D\beta_1}{Dt} - \lambda_4 c^2 \frac{D\beta_1}{Dt} = 0
\end{aligned}\right\} \qquad \text{(A17)}$$

Solving for λ_2, λ_3, and λ_4 in terms of λ_1 yields

$$\left.\begin{aligned}
\lambda_2 &= -\lambda_1 \frac{\dfrac{\partial \beta_1}{\partial r}}{\dfrac{D\beta_1}{Dt}} \\
\lambda_3 &= -\lambda_1 \frac{\dfrac{\partial \beta_1}{\partial z}}{\dfrac{D\beta_1}{Dt}} \\
\lambda_4 &= \frac{\lambda_1}{c^2}
\end{aligned}\right\} \qquad \text{(A18)}$$

From equations (A11) and (A13)

$$\left.\begin{aligned}
\frac{\dfrac{\partial \beta_1}{\partial r}}{\dfrac{D\beta_1}{Dt}} &= -\frac{\cos\theta}{c} \\
\frac{\dfrac{\partial \beta_1}{\partial z}}{\dfrac{D\beta_1}{Dt}} &= -\frac{\sin\theta}{c}
\end{aligned}\right\} \qquad \text{(A19)}$$

APPENDIX A

The negative sign results from the choice of reference for θ; therefore,

$$\left.\begin{aligned} \lambda_2 &= \frac{\lambda_1}{c}\cos\theta \\ \lambda_3 &= \frac{\lambda_1}{c}\sin\theta \\ \lambda_4 &= \frac{\lambda_1}{c^2} \end{aligned}\right\} \tag{A20}$$

By using equations (A20) for the λ's, the compatibility equation is determined from the sum of the weighted equations (1a) to (1d) as follows:

$$\lambda_1\left[\frac{D\rho}{Dt} + \rho\left(\frac{\partial u}{\partial r} + \frac{\partial v}{\partial z} + \frac{u}{r}\right)\right] + \frac{\lambda_1}{c}\left(\rho\frac{Du}{Dt} + \frac{\partial p}{\partial r}\right)\cos\theta + \frac{\lambda_1}{c}\left(\rho\frac{Dv}{Dt} + \frac{\partial p}{\partial z}\right)\sin\theta + \frac{\lambda_1}{c^2}\left(\frac{Dp}{Dt} - c^2\frac{D\rho}{Dt}\right) = 0 \tag{A21}$$

Along a bicharacteristic the time derivative becomes

$$\begin{aligned} \frac{d}{dt} &= \frac{\partial}{\partial t} + \frac{\partial}{\partial r}\frac{dr}{dt} + \frac{\partial}{\partial z}\frac{dz}{dt} \\ &= \frac{\partial}{\partial t} + (u + c\cos\theta)\frac{\partial}{\partial r} + (v + c\sin\theta)\frac{\partial}{\partial z} \end{aligned} \tag{A22}$$

Substituting equation (A22) into equation (A21) and reducing gives the final simplified form of the compatibility relation as

$$dp + \rho c\, du\cos\theta + \rho c\, dv\sin\theta = -\rho c^2\left[\left(\frac{\partial u}{\partial r}\right)\sin^2\theta - \left(\frac{\partial u}{\partial z} + \frac{\partial v}{\partial r}\right)\sin\theta\cos\theta + \left(\frac{\partial v}{\partial z}\right)\cos^2\theta + \frac{u}{r}\right]dt \tag{A23}$$

APPENDIX B

NUMERICAL STABILITY

The stability of numerical solutions to partial differential equations has been of much concern over the past few years. For hyperbolic equations, stability is usually based on the Von Neumann criterion (ref. 10) or the Courant-Friedrichs-Lewy (CFL) condition (ref. 11). The Von Neumann criterion, although very powerful, is not directly applicable since it relies on matrices and linear equations in one independent variable. The CFL condition is also difficult to apply since it requires that the domain of dependence of the difference equations encompass the domain of dependence of the original partial differential equations (fig. 14). It is possible, however, to use certain qualitative measures of stability based on the CFL philosophy. A brief discussion is presented of the approach used in the present study.

Consider the domain of dependence of the partial differential equations in the $(t_o - h)$ plane as illustrated in figure 15(a). If the conoid is now approximated by the three bicharacteristics indicated by the triangular symbols, a domain of dependence of the difference equations may be defined (ref. 10). The domain of dependence of the difference equations is described by the convex hull of the base points used in the calculation. When only points 1, 2, and 3 are used, the convex hull is a triangle connecting the three points (dashed line).

For stability, according to the CFL conditions the triangle must encompass the circle. The maximum probability of encompassing the circle will naturally occur when points 1, 2, and 3 are equally spaced around the circle; this indicates that the three θ_i's should be chosen at $2\pi/3$ angular intervals. However, when only points 1, 2, and 3 are used, another problem arises from convergence considerations. Since convergence dictates that the points 1, 2, and 3 lie relatively close to the circle, the triangle will not encompass the circle and instabilities will exist. This problem must be eliminated by increasing the domain of dependence of the difference scheme by utilizing more points in the previous time plane.

In the method utilized in the present paper, the points 1, 2, and 3 are obtained by interpolation in the calculation grid in the $(t_o - h)$ plane. The original three points are replaced by the 12 grid points (circular symbols) which surround points 1, 2, and 3 and thus the domain of dependence is increased to that shown in figure 15(b). This enlarged domain then gives a greater probability of stability.

Since there has been no evidence of instability in the present results, the spreading of the bicharacteristics and the interpolation in the $(t_o - h)$ plane appear to have assisted greatly in assuring numerical stability.

REFERENCES

1. Amsden, Anthony A.: The Particle-in-Cell Method for the Calculation of the Dynamics of Compressible Fluids. LA-3466, Los Alamos Sci. Lab., Univ. of California, June 24, 1966.

2. Johnson, W. E.: OIL – A Continuous Two-Dimensional Eulerian Hydrodynamic Code. GAMD-5580-Revised (Contract DA-04-495-AMC-116(x)), Gen. Dyn. Corp., Jan. 7, 1965. (Available from DDC as AD 477240.)

3. Madden, Richard: The Application of the Method of Characteristics in Three Independent Variables to the Hypervelocity Impact Problem. Ph. D. Thesis, Virginia Polytech. Inst., 1967.

4. Tillotson, J. H.: Metallic Equations of State for Hypervelocity Impact. GA-3216 (Contract AF 29(601)-4759), Gen. Dyn., July 18, 1962.

5. Elliott, L. A.: Shock Fronts in Two-Dimensional Flow. Proc. Roy. Soc. (London), ser. A, vol. 267, no. 1331, June 5, 1962, pp. 558-565.

6. Courant, R.; and Hilbert, D.: Methods of Mathematical Physics. Vol. II. Interscience Publ., c.1962.

7. Abbott, Michael B.: An Introduction to the Method of Characteristics. Amer. Elsevier Pub. Co., Inc., c.1966.

8. Von Mises, Richard: Mathematical Theory of Compressible Fluid Flow. Academic Press, Inc., 1958.

9. Crandall, Stephen H.: Engineering Analysis. McGraw-Hill Book Co., Inc., 1956.

10. Heie, H.; and Leigh, D. C.: Numerical Stability of Hyperbolic Equations in Three Independent Variables. AIAA J., vol. 3, no. 6, June 1965, pp. 1099-1103.

11. Courant R.; Friedrichs, K.; and Lewy, H.: Über die partiellen Differenzengleichungen der mathematischen Physik. Math. Ann., vol. 100, 1928, pp. 32-74.

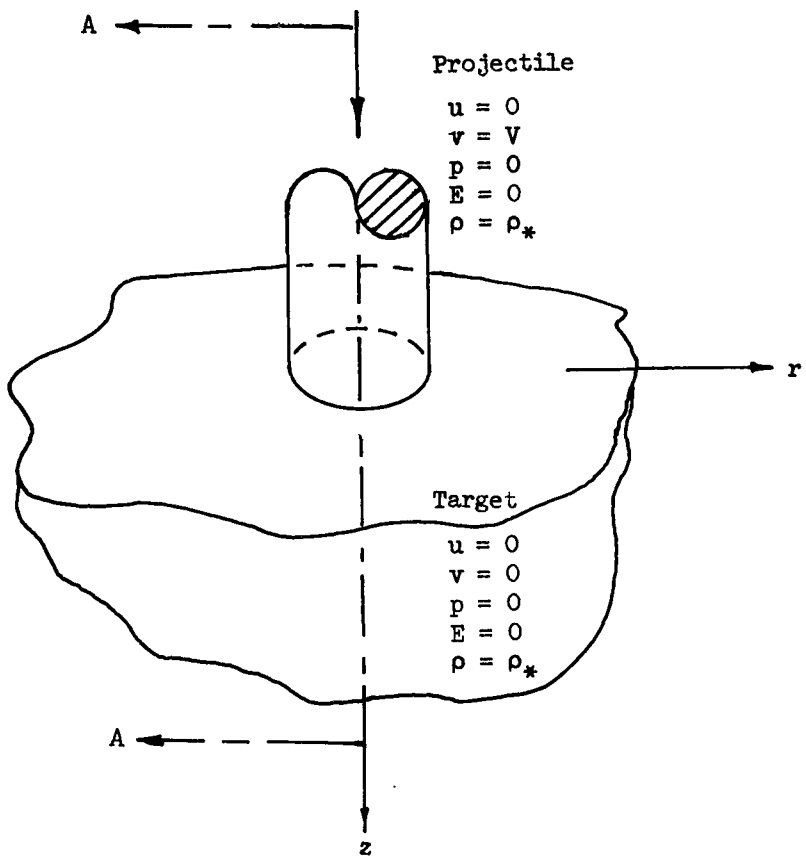

(a) Initial conditions.

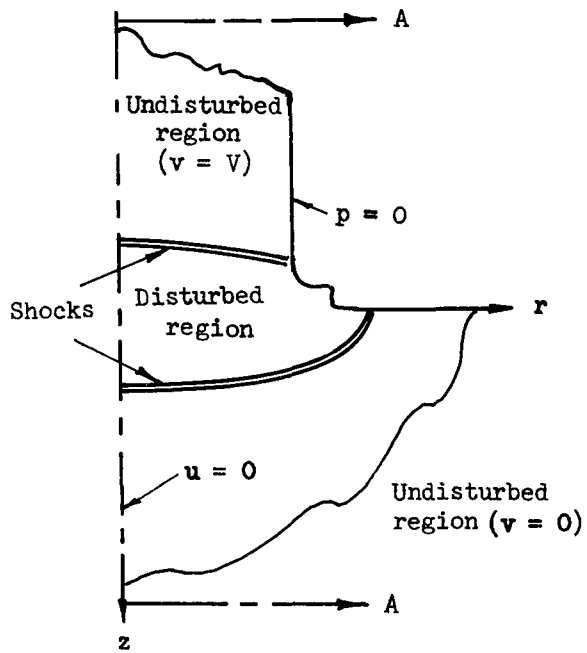

(b) Boundary conditions.

Figure 1.- Initial and boundary conditions.

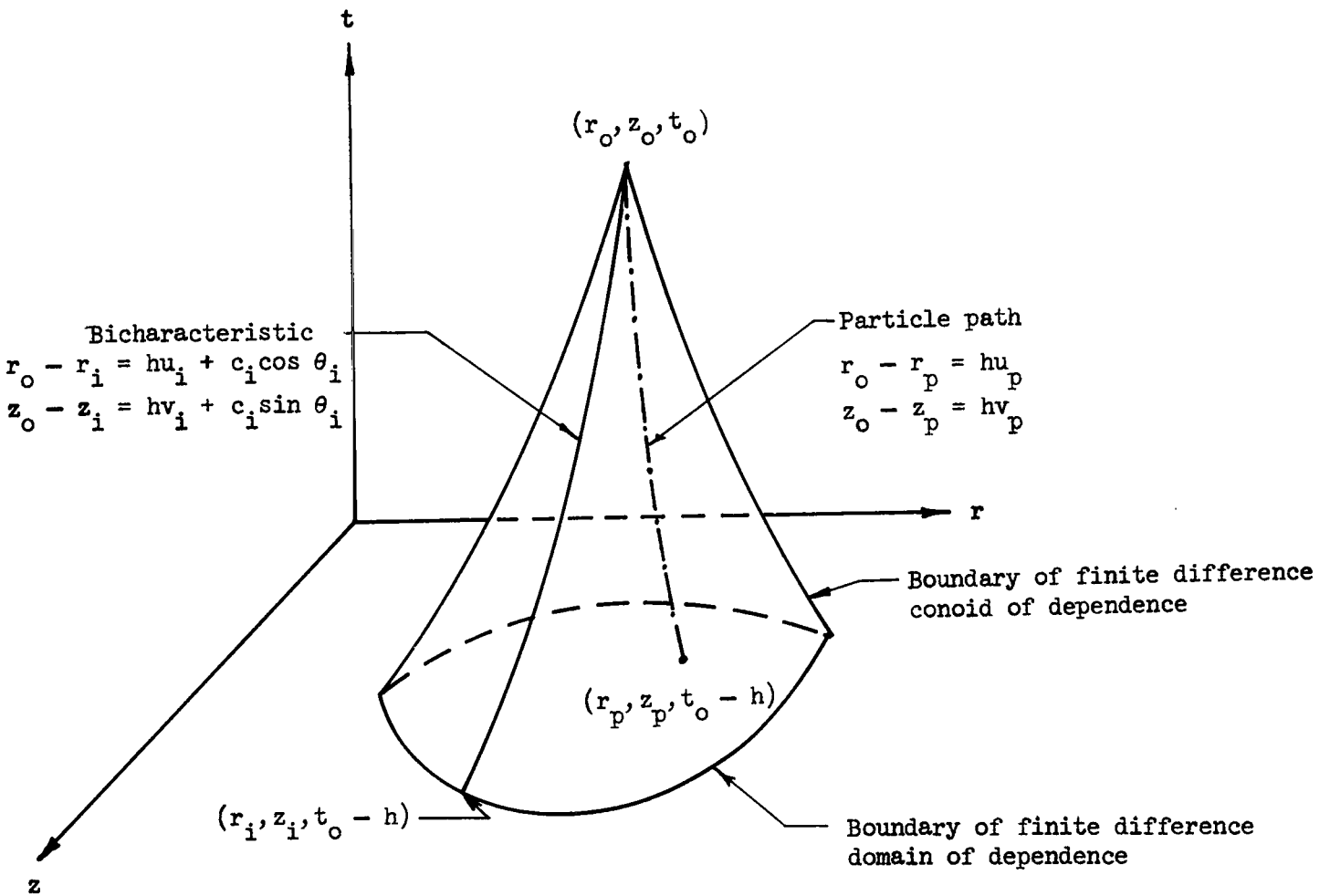

Figure 2.- Conoid of dependence for finite difference equations.

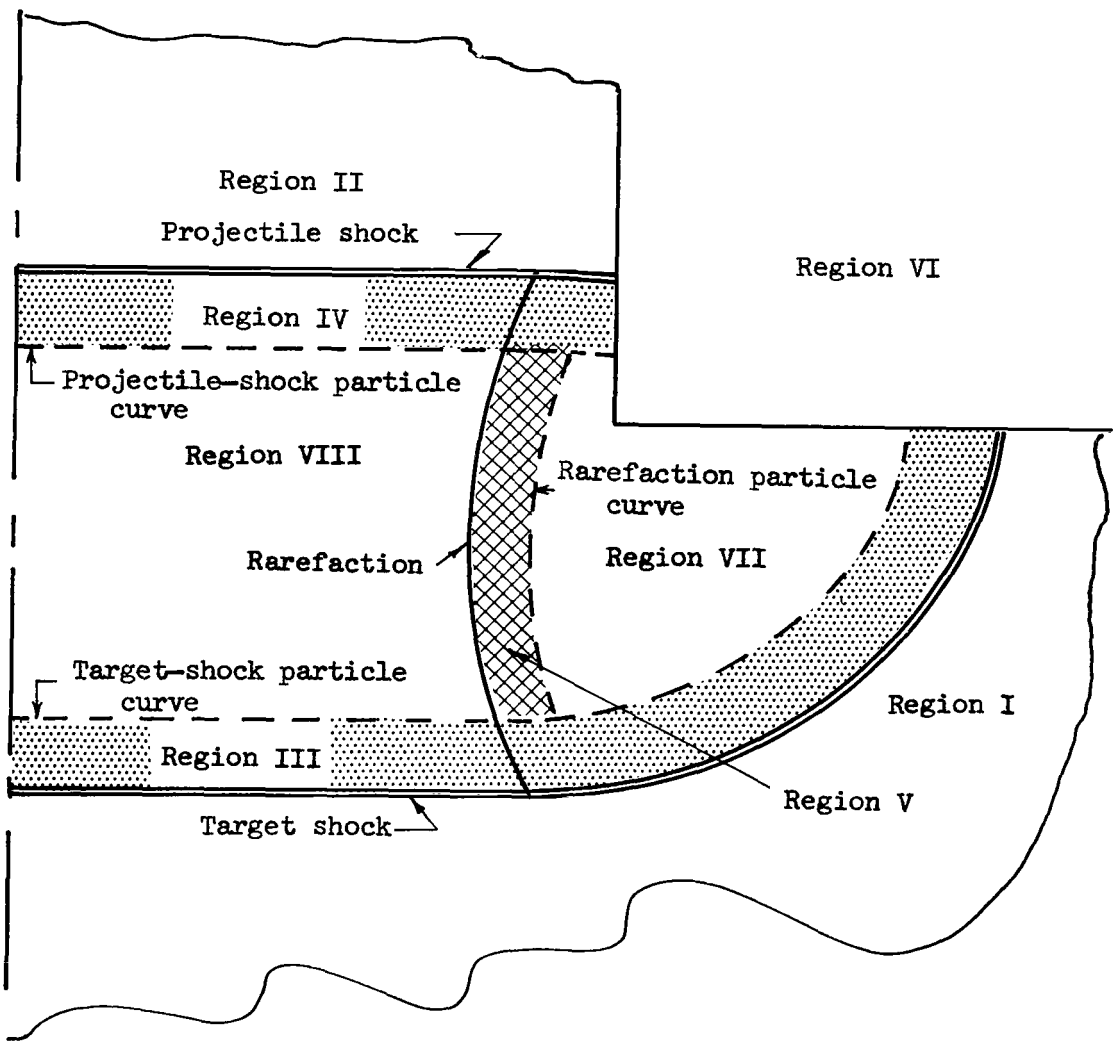

Figure 3.- Regions in the flow field.

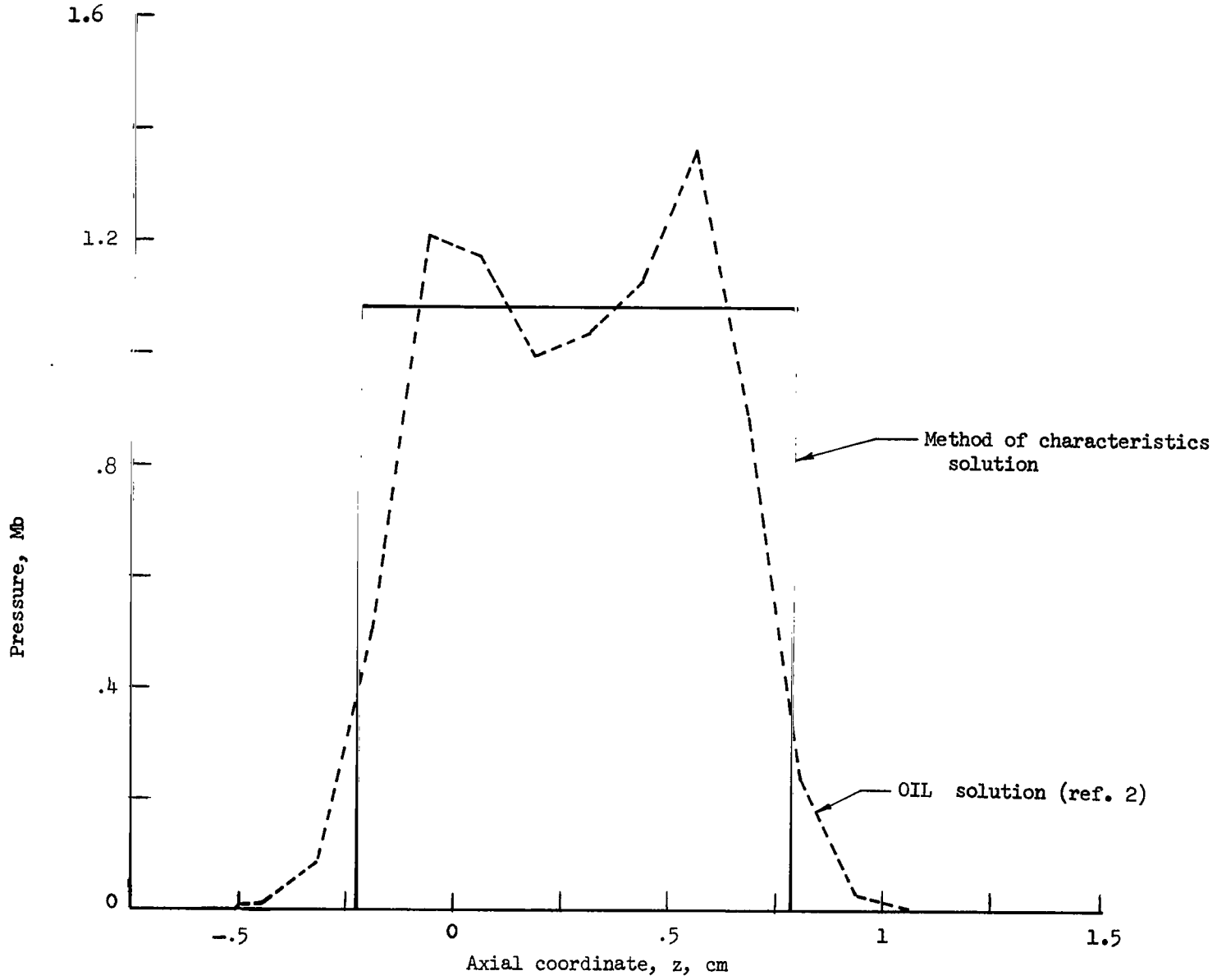

Figure 4.- Pressure on the axis of symmetry at T = 0.74 μs for the example impact problem. (1 Mb = 100 GN/m^2.)

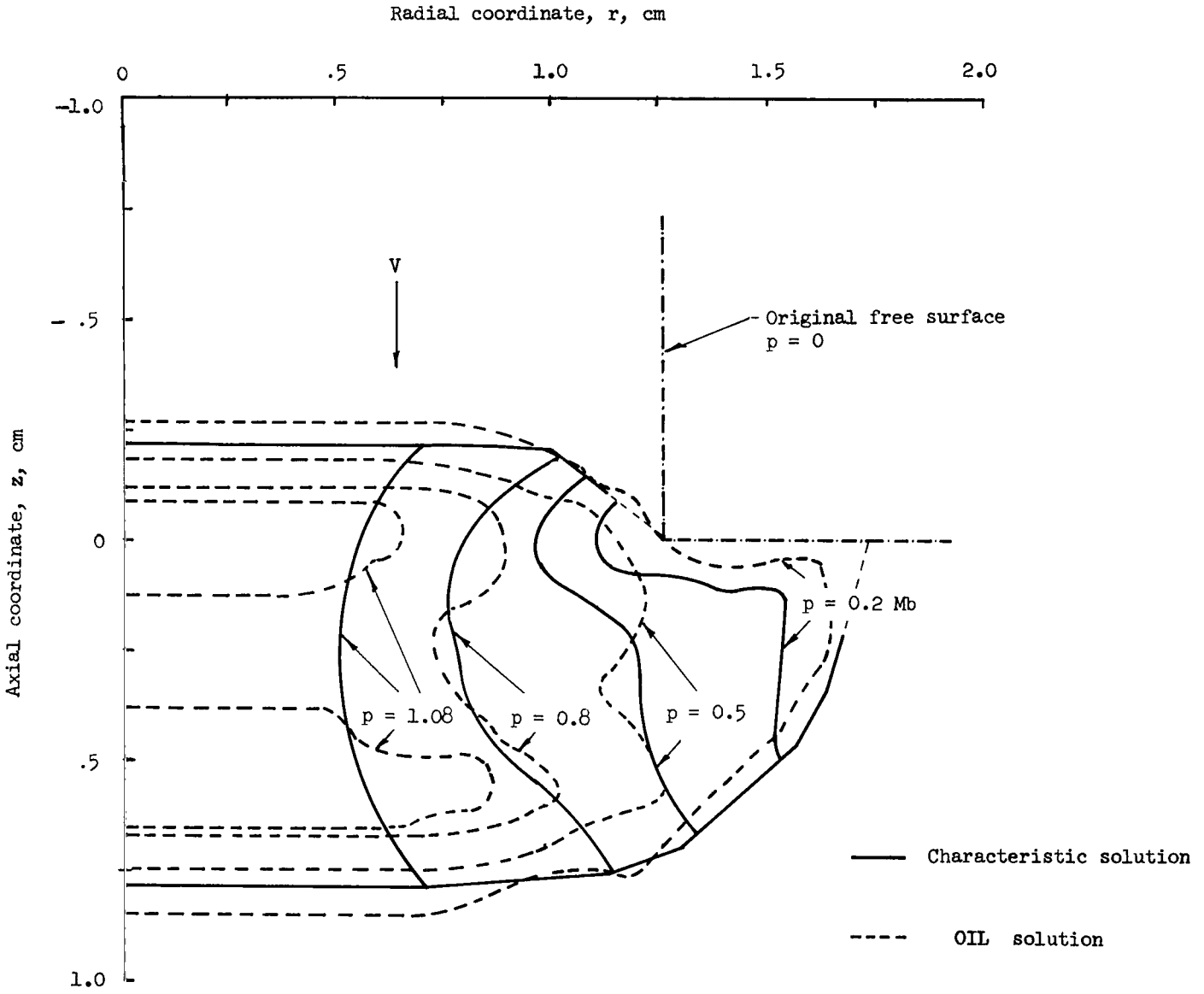

Figure 5.- Isobars from the characteristic and OIL solutions at T = 0.74 μs for ; impact problem. (1 Mb = 100 GN/m2.)

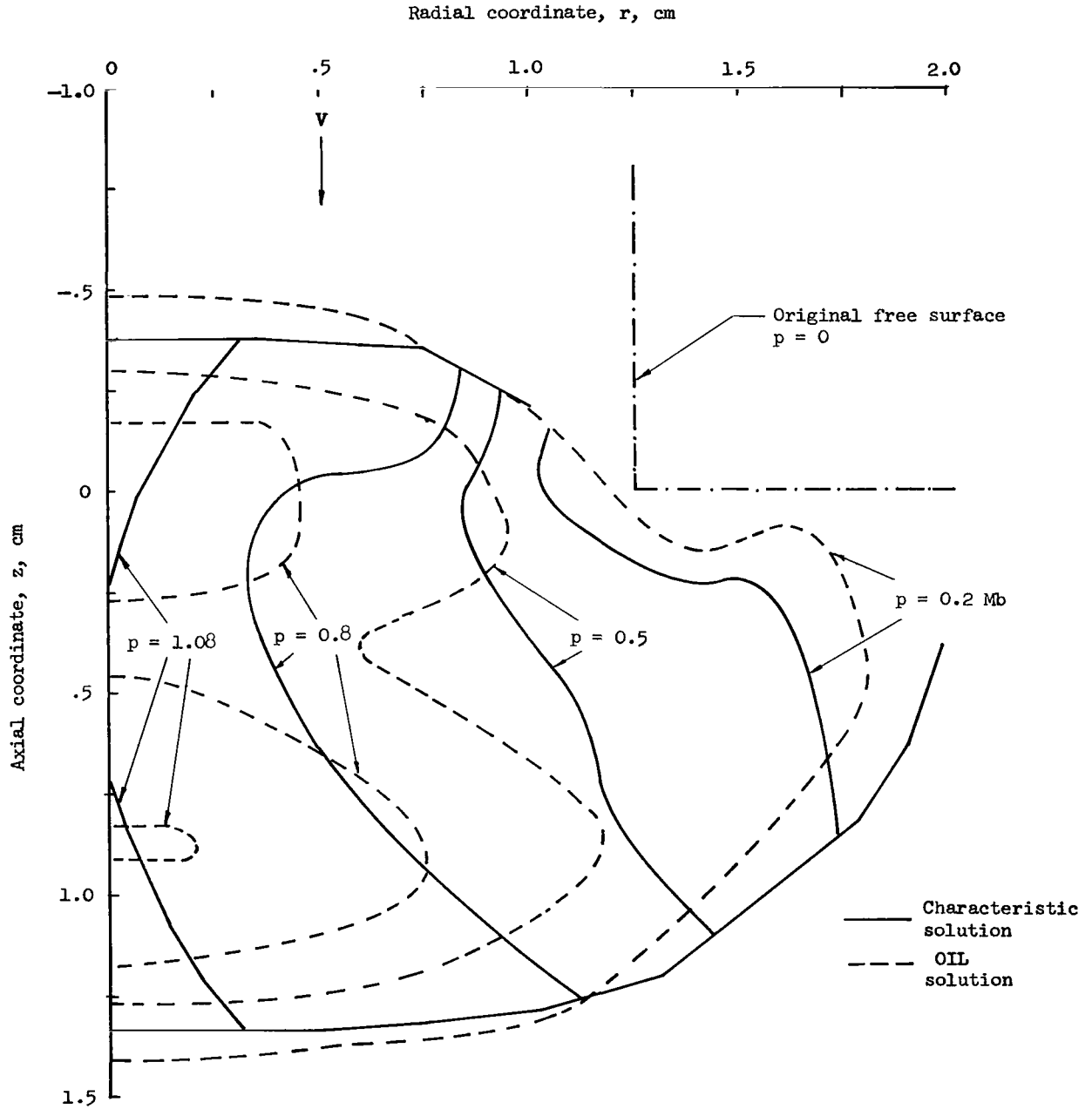

Figure 6.- Isobars from the characteristic and OIL solutions at T = 1.26 μs for the example impact problem. (1 Mb = 100 GN/m^2.)

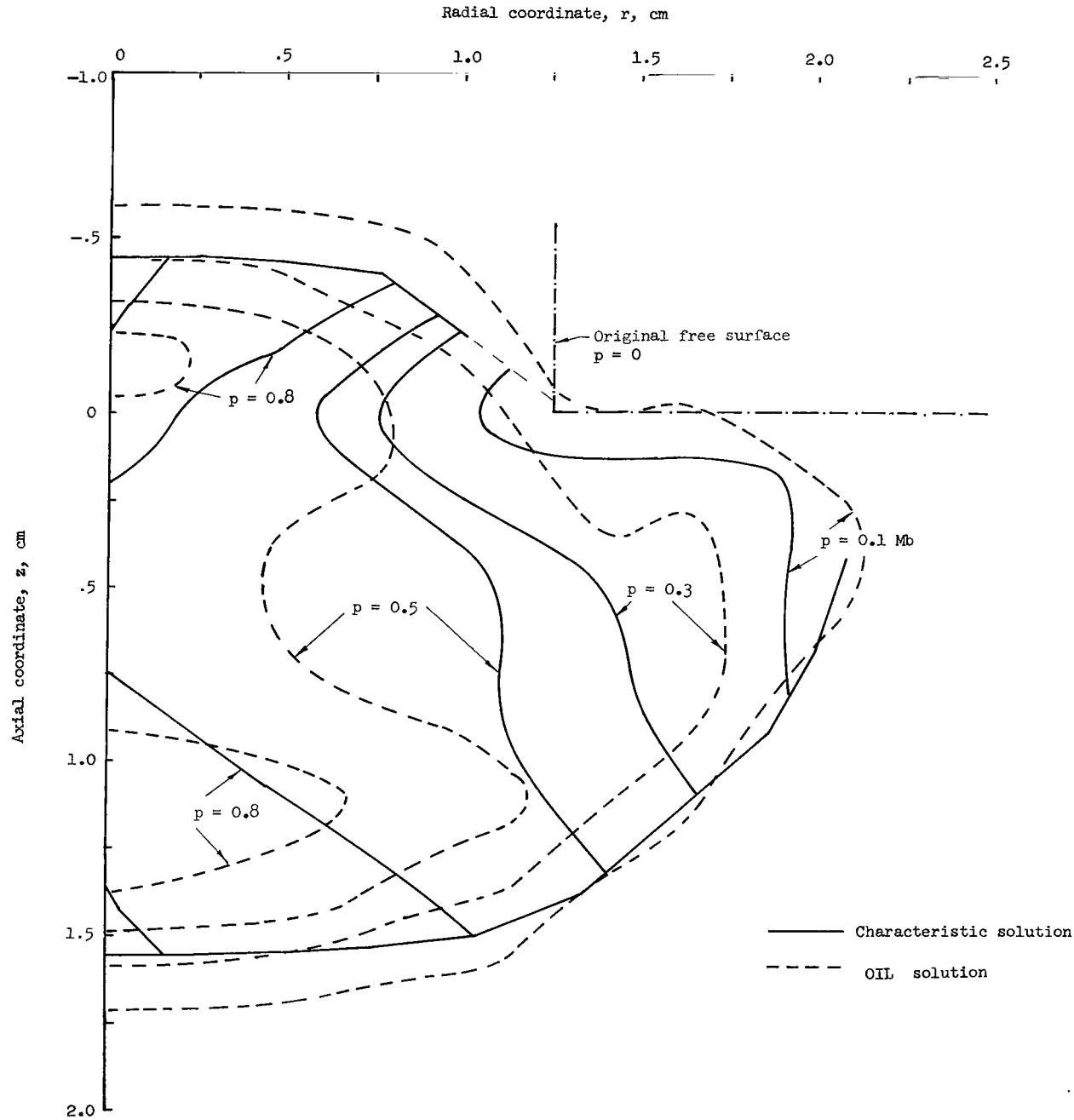

Figure 7.- Isobars from the characteristic and OIL solutions at T = 1.5 μs for the example impact problem. (1 Mb = 100 GN/m^2.)

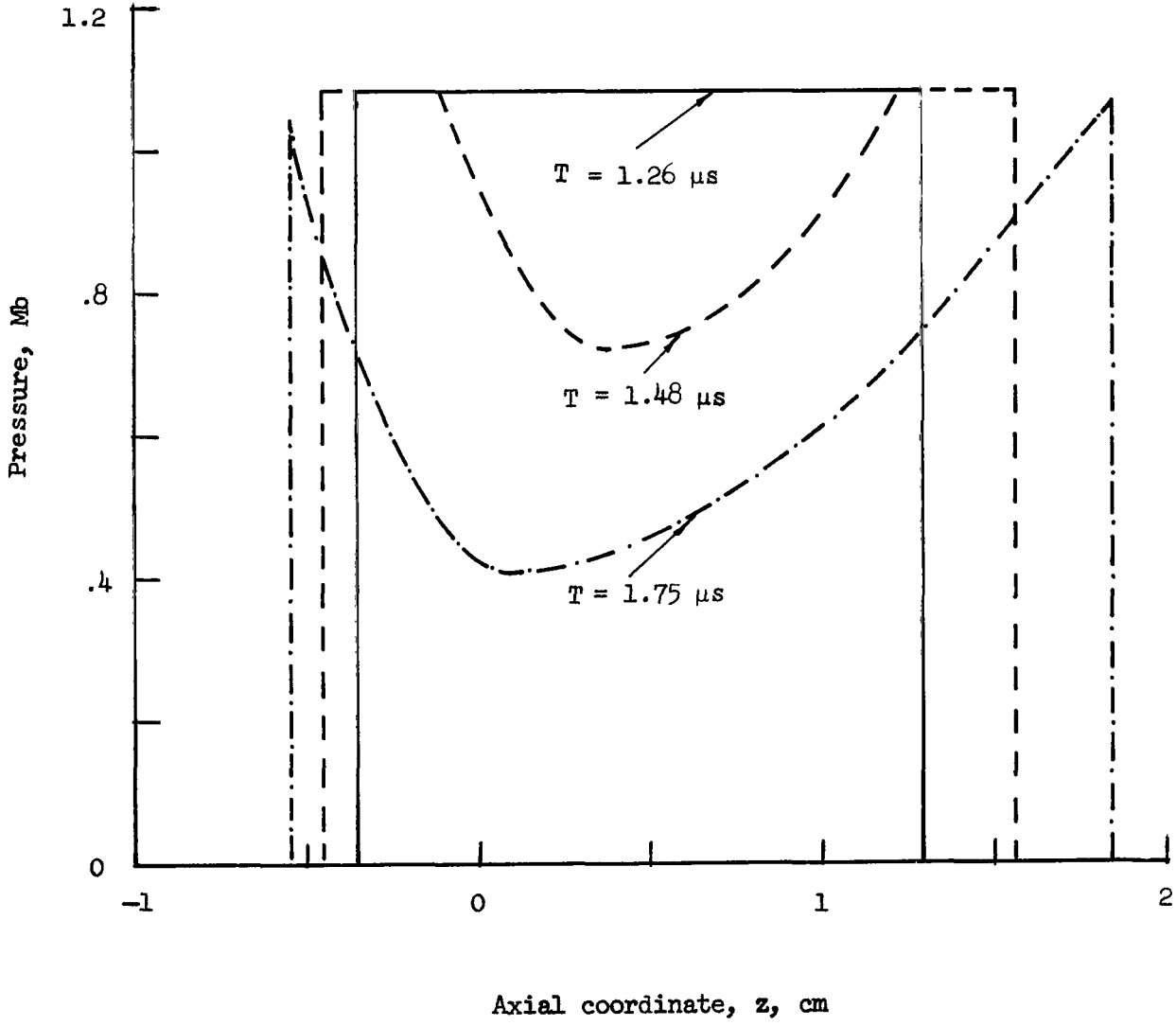

Figure 8.- Pressure on the axis of symmetry at various times as predicted by the characteristic method for the example impact problem.

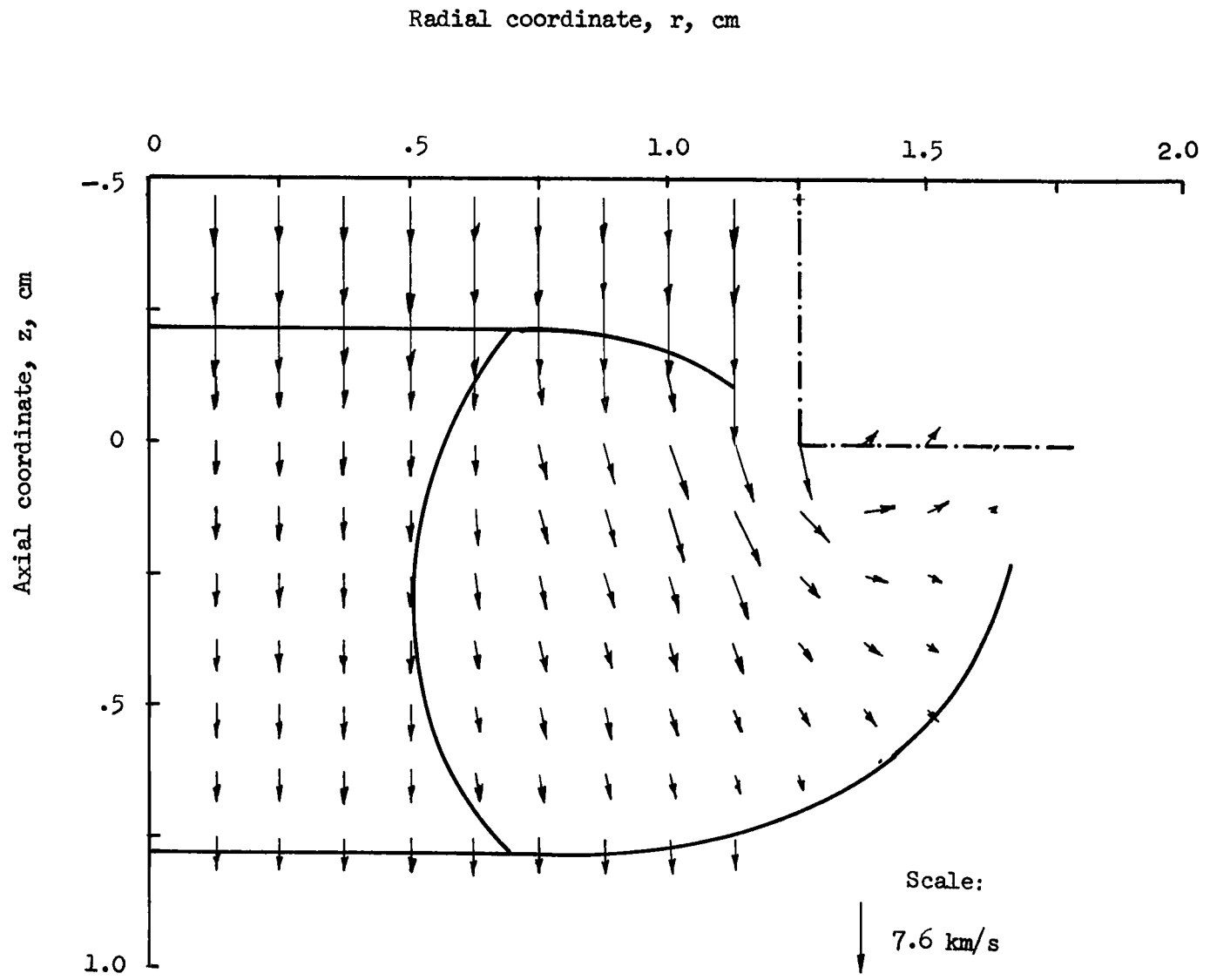

Figure 9.- Velocity vector field as predicted by the characteristic method at T = 0.74 μs for the example impact problem.

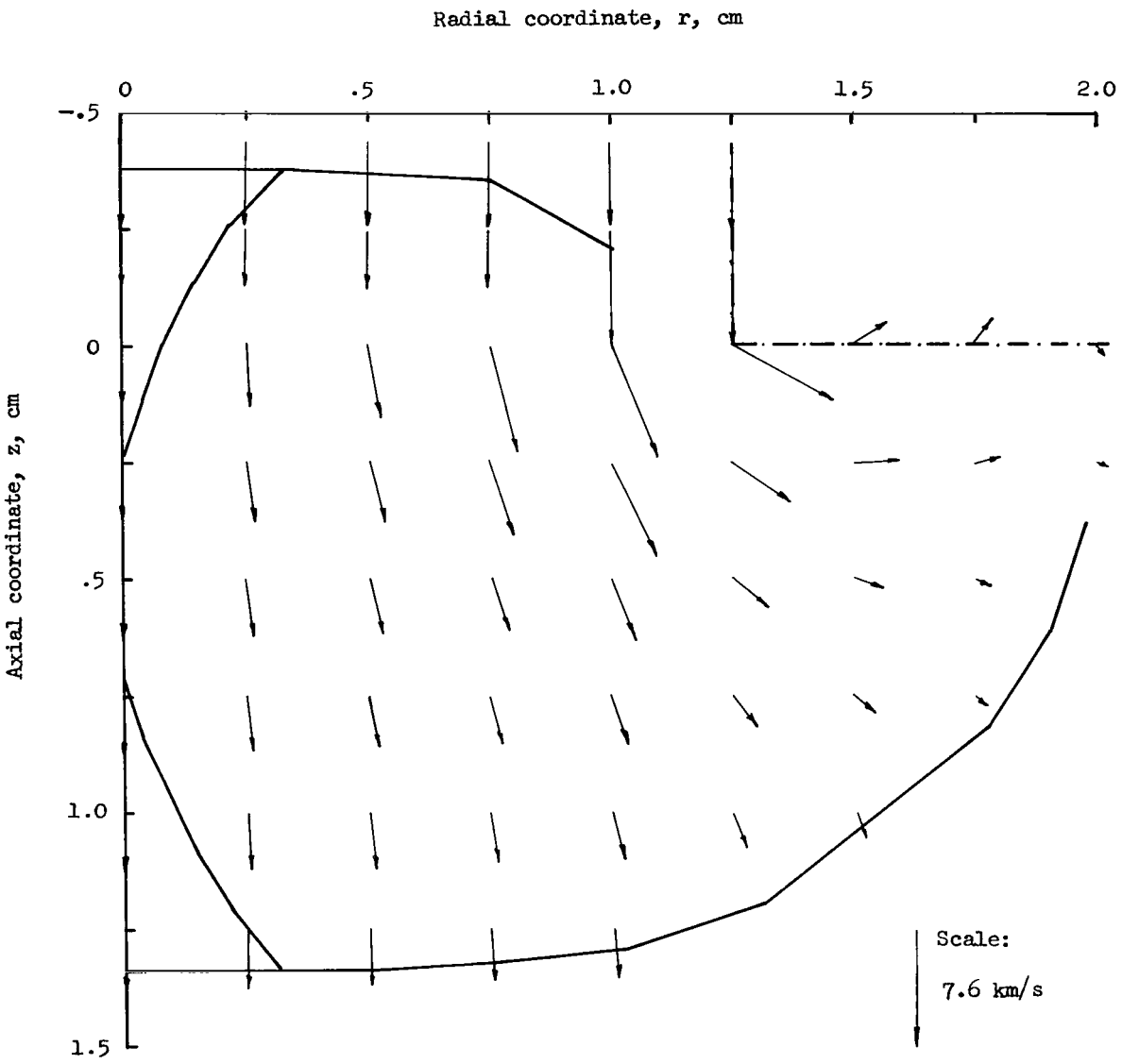

Figure 10.- Velocity vector field as predicted by the characteristic method at T = 1.26 μs for the example impact problem.

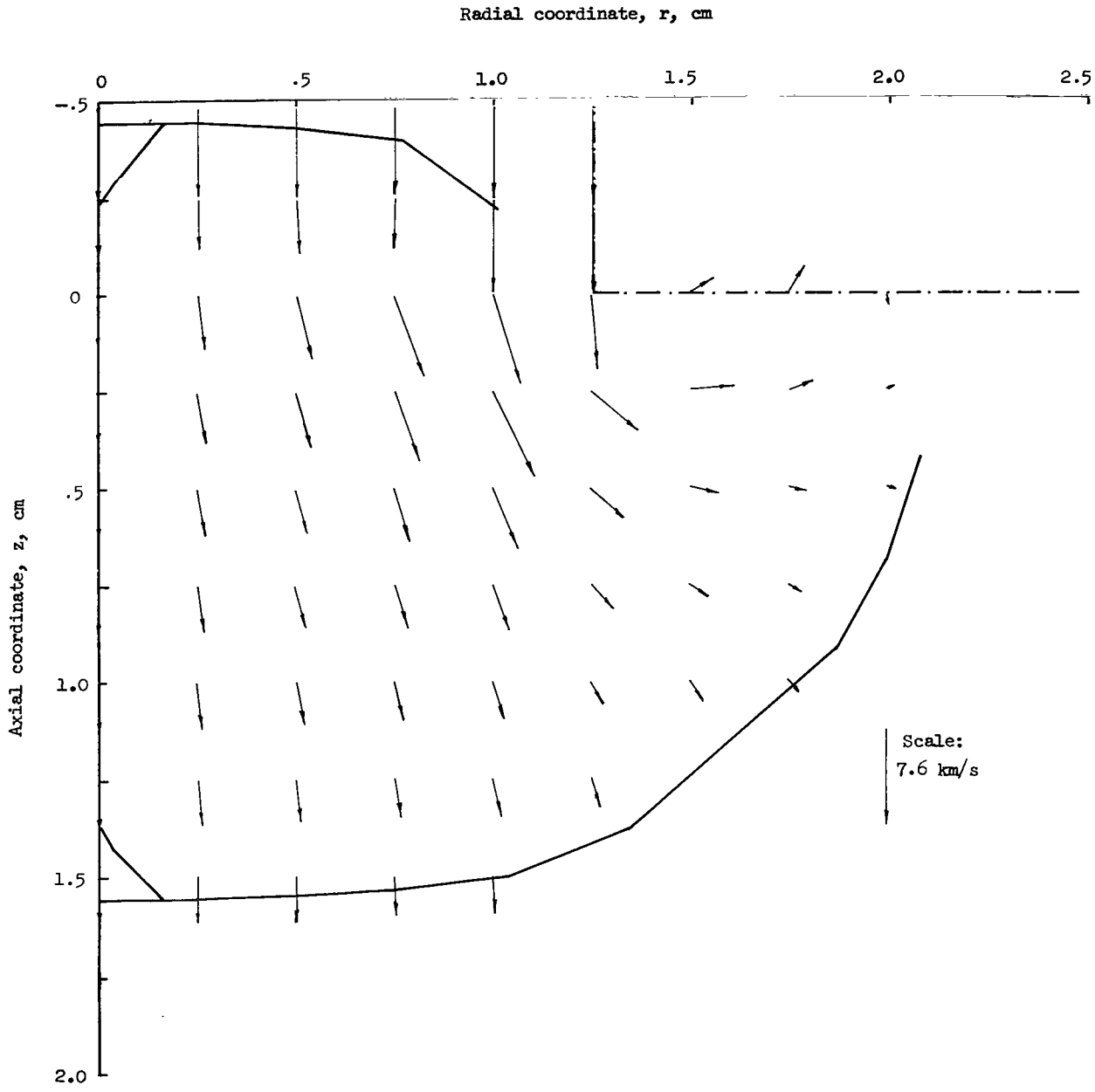

Figure 11.- Velocity vector field as predicted by the characteristic method at T = 1.5 μs for the example impact problem.

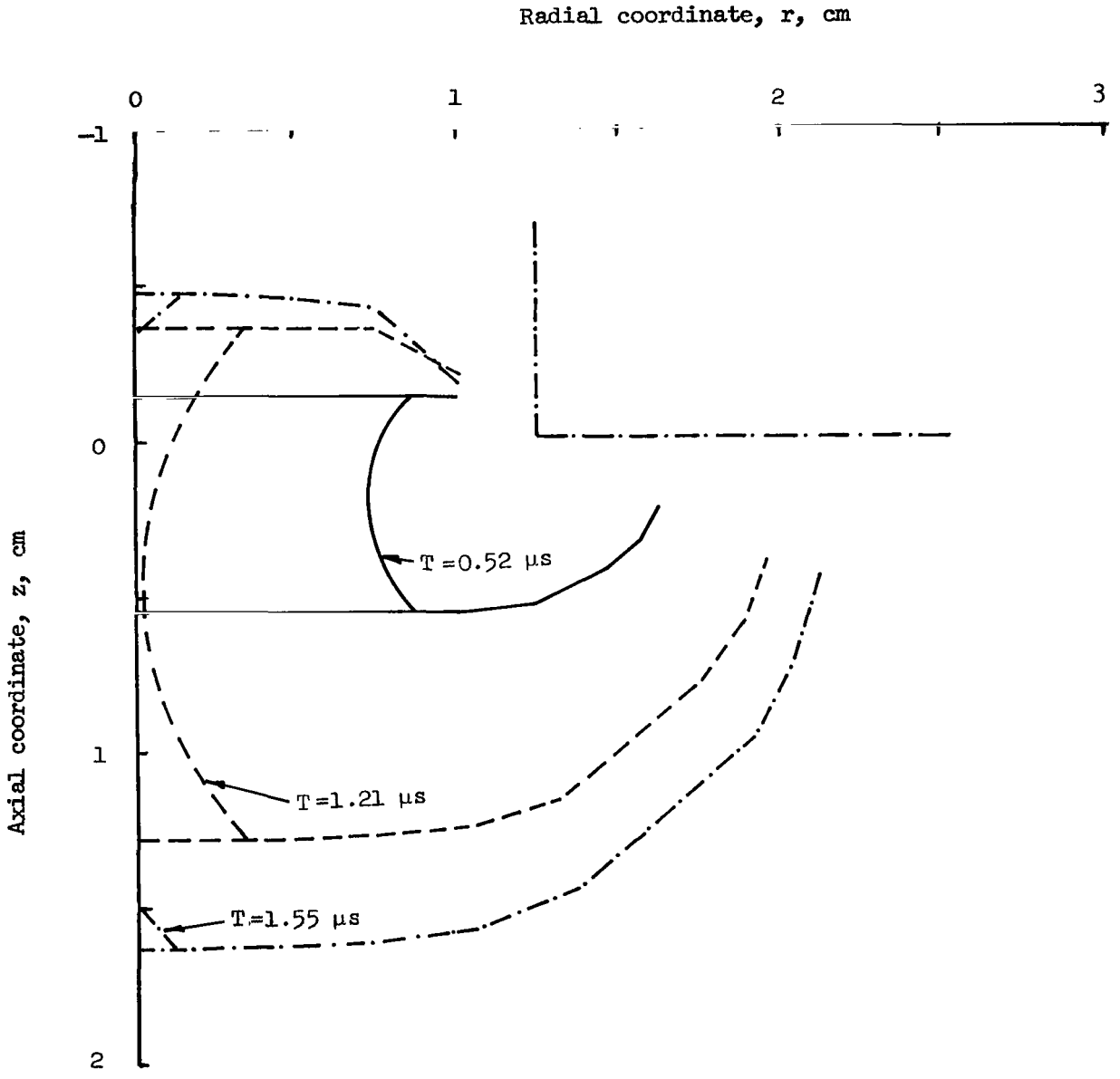

Figure 12.- Locations of the discontinuities as a function of time as predicted by the characteristic method for the example impact problem.

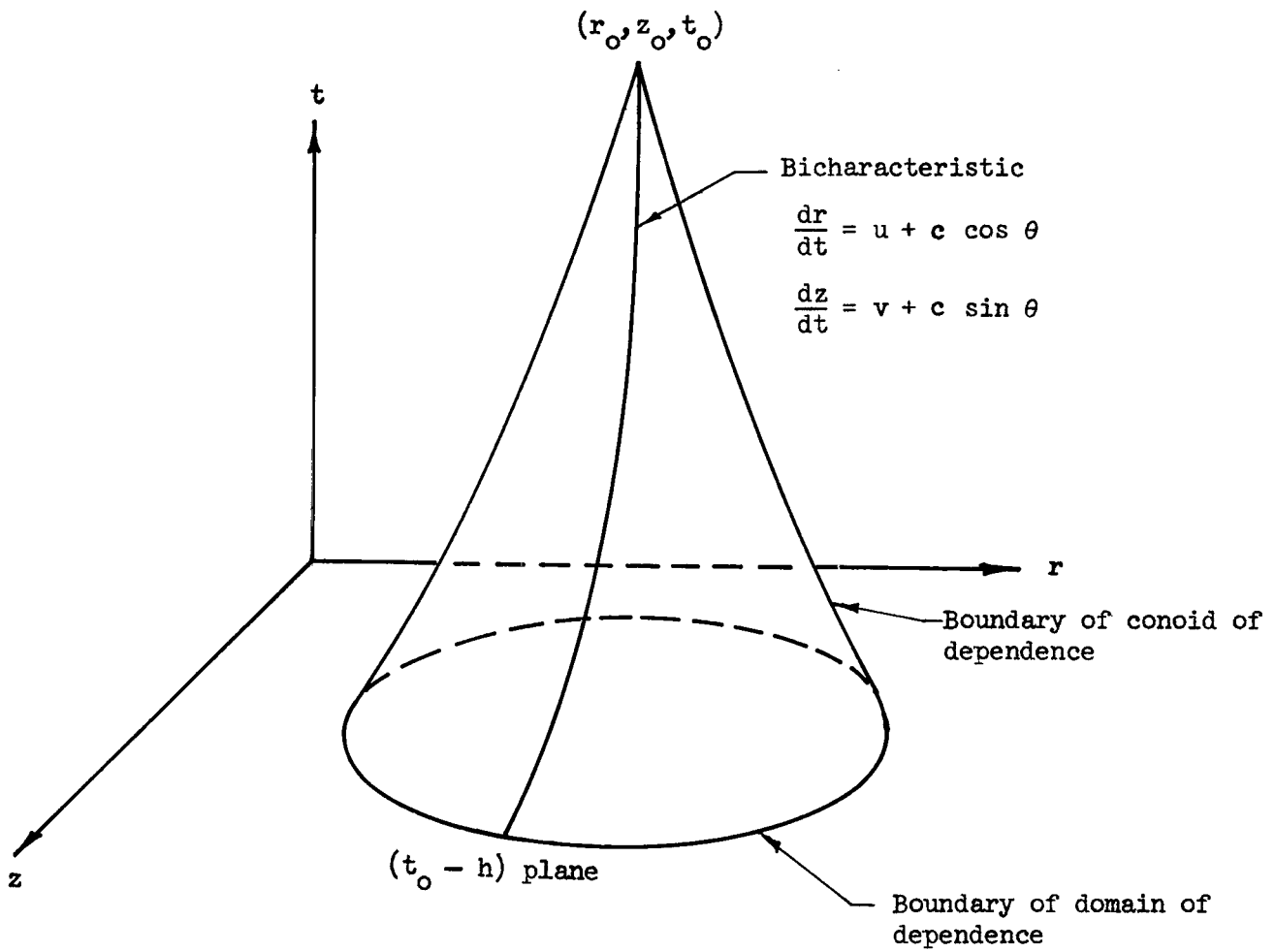

Figure 13.- Conoid of dependence.

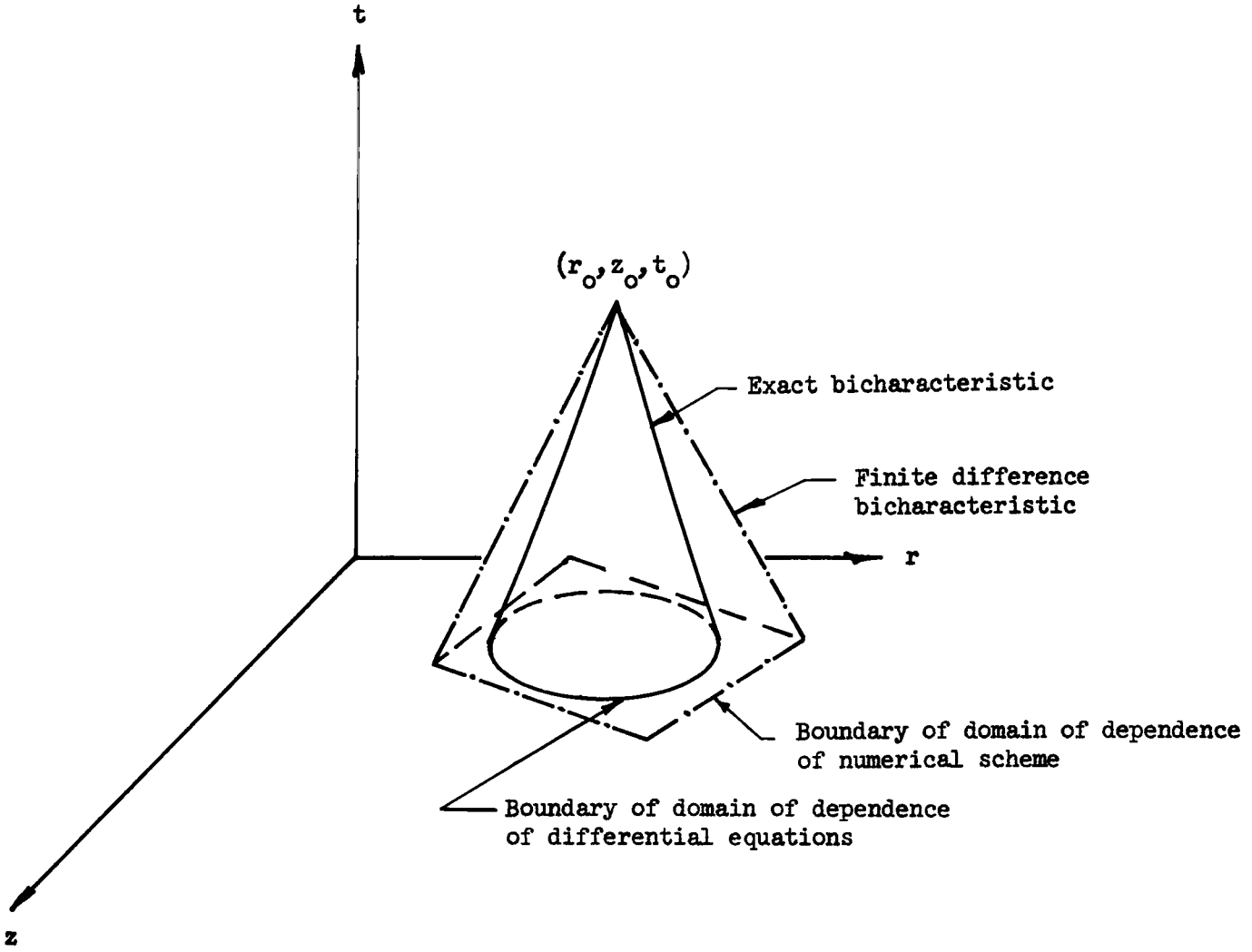

Figure 14.- Diagram of stable numerical scheme.

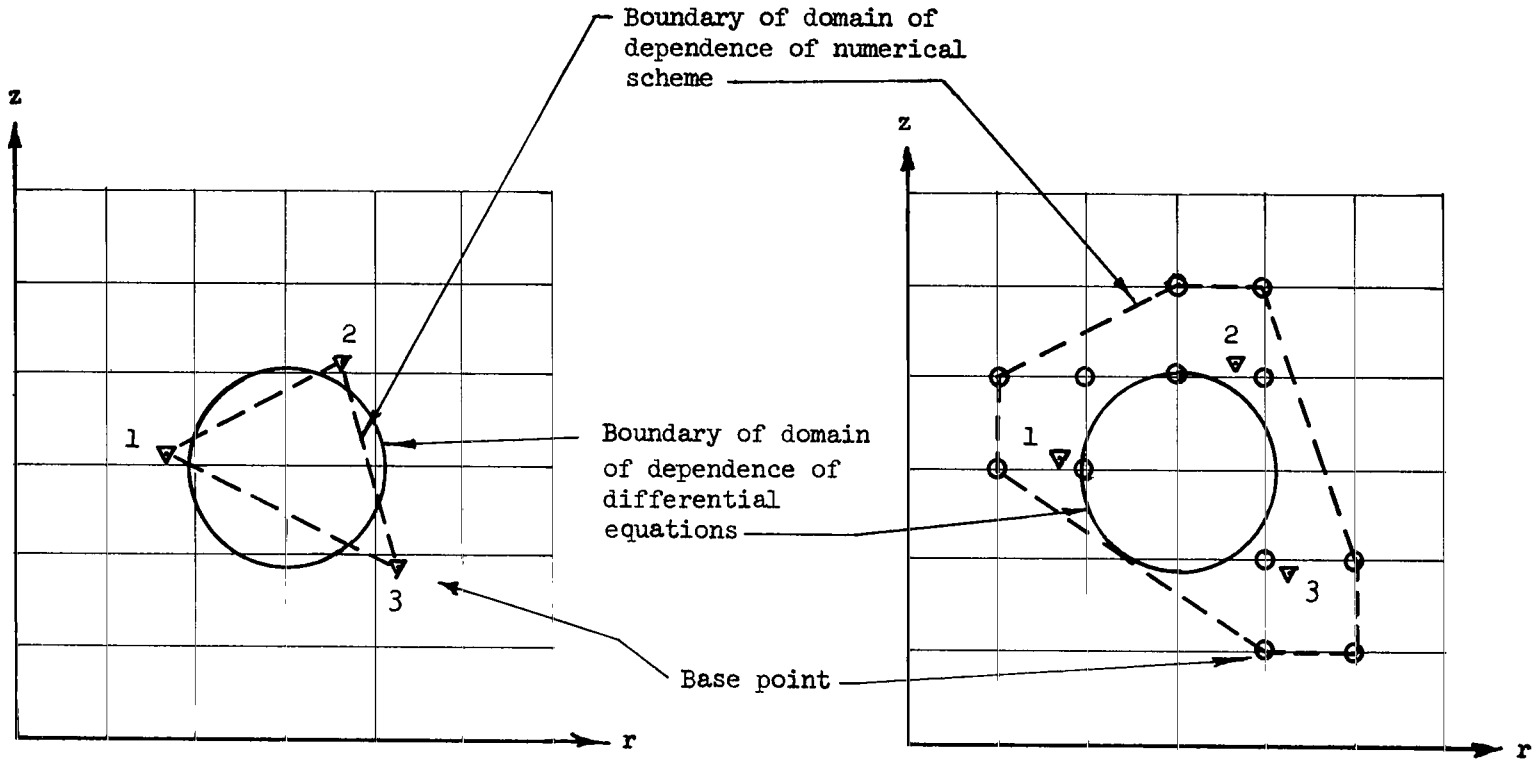

(a) Domain without interpolation.

(b) Domain with interpolation.

Figure 15.- Domains of dependence in the (t_0 - h) plane.

"The aeronautical and space activities of the United States shall be conducted so as to contribute . . . to the expansion of human knowledge of phenomena in the atmosphere and space. The Administration shall provide for the widest practicable and appropriate dissemination of information concerning its activities and the results thereof."

—NATIONAL AERONAUTICS AND SPACE ACT OF 1958

NASA SCIENTIFIC AND TECHNICAL PUBLICATIONS

TECHNICAL REPORTS: Scientific and technical information considered important, complete, and a lasting contribution to existing knowledge.

TECHNICAL NOTES: Information less broad in scope but nevertheless of importance as a contribution to existing knowledge.

TECHNICAL MEMORANDUMS: Information receiving limited distribution because of preliminary data, security classification, or other reasons.

CONTRACTOR REPORTS: Scientific and technical information generated under a NASA contract or grant and considered an important contribution to existing knowledge.

TECHNICAL TRANSLATIONS: Information published in a foreign language considered to merit NASA distribution in English.

SPECIAL PUBLICATIONS: Information derived from or of value to NASA activities. Publications include conference proceedings, monographs, data compilations, handbooks, sourcebooks, and special bibliographies.

TECHNOLOGY UTILIZATION PUBLICATIONS: Information on technology used by NASA that may be of particular interest in commercial and other non-aerospace applications. Publications include Tech Briefs, Technology Utilization Reports and Notes, and Technology Surveys.

Details on the availability of these publications may be obtained from:

SCIENTIFIC AND TECHNICAL INFORMATION DIVISION

NATIONAL AERONAUTICS AND SPACE ADMINISTRATION

Washington, D.C. 20546